Wireless Charger for Hand-held Mobile Devices

EE3L11 - BSc Project: Final Thesis

July 27, 2018

L. Marting - 4445600
J.P. van der Velden - 4469976

Technische Universiteit Delft

TU Delft Delft University of Technology

Challenge the future

Preface

This thesis is part of the Bachelor Graduation Project for Electrical Engineering at the TU Delft. The project as a whole consists of two groups. The members of the other group are Nandor Toth and Jordy van der Horst. The group was tasked with designing a wireless power transfer system. We design and test the transmitter, while the other group designs and tests the receiver. Further details on the whole system are addressed in the introduction.

We would like to thank our supervisors Marco Pelk, Masoud Babaie and Morteza Alavi for gladly giving us feedback every week. The sharp eye of our supervisors kept us searching for the best solution and we felt encouraged to do more after our weekly meetings. Furthermore, we would like to thank Martin Schumacher for ordering the many, many parts we kindly requested. He even helped us with a late order and resolved an issue between Farnell and the TU Delft.

We hope you will find reading our bachelor thesis insightful and enjoyable. We are but humble bachelor students and we hope you may appreciate the results presented in this thesis. Enjoy!

Louis Marting
Joram van der Velden
Delft, July 27, 2018

Abstract

This thesis describes the design and prototyping results of a low power wireless power transfer (WPT) system. In particular the design and testing of a transmitter.

Firstly, existing research is discussed and it is found that a significant part of this discusses higher power transfer systems. Here lies the challenge for this thesis: to find an efficient way of transferring a low amount of power wirelessly, with a significant distance between the transmitter and the receiver. Also, existing WPT standards were investigated and their shortcomings are discussed.

Secondly, the design of the transmitter is discussed. It starts out with the fundamental and circuit theory behind wireless power transfer. With this, it is found that tuning capacitors can greatly increase the efficiency of the system. Next, the design of the components in the coupled coils system is discussed, with calculations on equivalent series resistance for different frequencies. Furthermore, the functional block diagram consists of an oscillator, gate driver and inverter circuit and its design choices are discussed. The design concludes with a frequency optimization and simulation results.

Lastly, the design has been built and tested. A transmitter efficiency of 93.4% has been reached at a coupling of around 0.1. This is at a distance of 20 millimeters. Further improvements may be done with the gate-driver. Control techniques may also prove beneficial for future work.

Contents

1 Introduction

Recently, wireless power transfer (WPT), and in particular wireless charging, has become more popular. Since the first idea by Nicola Tesla [1] and the first modern solution [2], wireless power transfer has made big leaps. A common example seen today is the wireless charging of smart-phones or smart-watches. Wireless charging works on the principle of creating a time varying electromagnetic field to transfer electrical energy over a distance. The aim is to design a WPT-transmitter-system for low power systems (5W). To find a starting point for the design, the current state-of-the-art technology is investigated.

1.1. State-of-the-art analysis

Two approaches stem from using a time varying electromagnetic field to transfer power. The first approach is radiative power transfer [3]. Microwaves are beamed over a long distance. The second is a non-radiative technique. A resonating magnetic field transfers power over an air gap [4]. In this thesis, the focus will be on the second approach.

Non-radiative transfer has several applications, the automotive industry would like to use the technology for high power wireless charging of cars [5][6]. Low power systems already are common, and have been for quite some time [7]. Two standards exist for wireless power transfer: Qi [8] and Airfuel [9]. The efficiency and distance is limited however. WPT-systems in lab conditions show results with efficiencies almost or as high as wired systems, or with greater distances, but these systems are not practical for consumer electronics. The coils/systems are too big and are not scalable [10][11].

1.1.1. Fundamental principals

Before the design of the circuit can be realized, first the fundamental principals of power transfer through coupled coils needs to be studied. Various aspects of basic coupled coil circuits are described in [12][13]. [14] and [15] show different ways to optimize a coupled circuit. [16] shows an application of the circuit for wireless power transfer in biomedical implants.

1.1.2. Design considerations

From the basic concept of wireless power transfer to the final design, the literature offers several methods and considerations in the design [17]. Alignment of the coils is of critical value to the efficiency of the system [18]. Solutions exist to minimize the misalignment losses [19]. More general, the variation of the coupling and of the power delivered to the load give rise to problems. The efficiency decreases rapidly with a mismatched load, or a coupling too high or too low. Both are related, and are hard to control or counteract [20][21].
Lastly, inverter circuits are widely used to power oscillating circuits. From high power systems and low switching times, to high frequency RF inverters. The main goal to achieve in inverters is minimizing losses [22]. Several techniques do exist in reducing losses [23][24]. Examples are zero voltage switching, soft switching or using different topologies [25][26][27]. Main factors in calculating losses are the

switching times, internal resistances of the MOSFETs and gate capacitance of the MOSFETs. Note that with low power, not all principles discussed in the literature are applicable to this setup.

1.2. Problem definition

Wireless charging is commonplace in many hand-held mobile devices. Simple design, universality and convenience are the drivers behind this technology. It enables devices to be sealed, wireless systems have a better longevity compared to wires and the system is universal in all devices. Nevertheless, conventional charging methods still have the edge when it comes to power transfer efficiency, distance for delivering power and, in general, the maturity of conventional charging methods make it an attractive alternative.

The WPT-standard for most smart-devices is the Qi standard, but the implementation requires sophisticated protocols and hardware. The efficiency of such systems lies around 60-70% and the maximum transfer distance is 1cm. In this thesis we aim to achieve a solution for a WPT-system with up to 80% efficiency and a transfer distance of several centimeters. The transfer distance will be around the same dimension as the intended coil size.

1.2.1. Synopsis

The task discussed in this thesis is the design of the transmitter. Considering the minimum requirements mentioned above, and the losses of the airgap and receiver. The aim is to have a transmitter efficiency of 90%.
The efficiency is measured from a DC source to the transmitter coil. A certain loss is to be expected trough the airgap and is not considered part of the efficiency. The system is implemented by using an inverter that powers the coils in an oscillating manner and the necessary control for doing so. The formal constraints of the system are set in Chapter 2.

2

Programme of requirements

To formally state the bounds of this thesis, a programme of requirements (PoR) is given. The product is intended for the consumer market, this will imply several standards, mainly health and safety.

2.1. Functional requirements

1. The system shall deliver 5 watts to a 5 ohm load
2. The system shall be powered by a DC source
3. The system must generate a frequency internally
4. The system must deliver >5 watts to a coil used for wireless power transfer at the chosen frequency

2.2. System requirements

1. The physical distance between the transmitter and receiver must exceed two centimeters
2. The frequency must be between 80 and 300 kHz
3. The efficiency over the system from source to load should at least exceed 70%
4. The efficiency of the transmitter should at least exceed 90%
5. The device should be able to fit into 5x10x4 cm box

2.3. Ecological requirements

1. The system must adhere to the dutch health and safety standards, in particular adhere to magnetic exposure requirements [28]

3

Design

In this chapter, the reasoning for the design of the transmitter is given, constrained by the Programme of Requirements (PoR). Firstly, the theoretical background is given and an equivalent circuit for wireless power transfer is derived. After that a functional design is presented. The parts consisting of the functional design are elaborated upon and the choices for the design are stated. The design is validated with equations and simulations. Lastly the final design is presented.

3.1. Theory of wireless power transfer

The whole basis on which wireless power transfer works is because of magnetic fields generated by the coils in the transmitter can be captured by coils in the receiver. These fields carry energy, this energy is captured by the receiver coils. A more formal definition of this phenomenon is given by Faraday's law.

Faraday's law is stated as follows:

$$\mathcal{E} = N \cdot -\frac{d\Phi_B}{dt} \quad [\text{V}] \tag{3.1}$$

A changing magnetic field flux (Φ_B) though the surface of the receiver coil with N turns will induce a voltage (the electromotive force ($\mathcal{E}$)) at the terminals of the receiver. $\mathcal{E}$ will be opposite to the change in the magnetic flux. When a load is connected, a current will flow due to the voltage $\mathcal{E}$ over the load. The result is power delivered to a load.

A coil, or an inductor is defined as follows:

$$L = \frac{\Phi_B}{I} \quad [\text{H}] \tag{3.2}$$

Where L is the inductance of a coil, I is the current through the coil and Φ_B is the magnetic flux induced due to that current. Given these two theoretical bases, two coupled coils can be used, powered with a changing current and have shared flux between the coils.

3.1.1. Circuit theory

Calculating the flux the two coils share requires sophisticated modeling of the fields. A more practical approach comes from circuit theory. In circuit theory, two coupled coils are shown as a two-port. Figure 3.1 shows a two port with coils L_1 and L_2.

The relations between the phasor voltages and currents for the coils in Figure 3.1 are given as follows:

$$\begin{aligned} \mathbf{V_1} &= j\omega L_1 \cdot \mathbf{I_1} + j\omega M \cdot \mathbf{I_2} \\ \mathbf{V_2} &= j\omega M \cdot \mathbf{I_1} + j\omega L_2 \cdot \mathbf{I_2} \end{aligned} \tag{3.3}$$

Where the mutual inductance M is defined as:

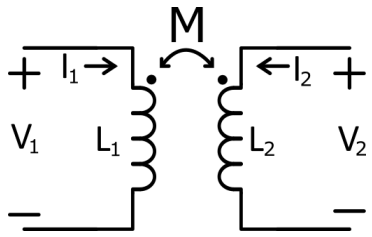

Figure 3.1: Two-port network of coupled coils

$$M = k\sqrt{L_1 L_2}, \quad 0 \leq k \leq 1 \quad [\mathrm{H}] \tag{3.4}$$

The mutual inductance M is a measure for how much electromotive force $\mathcal{E}$ is induced at a certain coupling factor k. k therefore defines the amount of the induced field that the coils can capture. For example, imagine that coil L_2 is connected to an open terminal, then Equation 3.3 is simplified to the following:

$$\begin{aligned} \mathbf{V_1} &= j\omega L_1 \cdot \mathbf{I_1} \\ \mathbf{V_2} &= j\omega M \cdot \mathbf{I_1} \end{aligned} \tag{3.5}$$

The induced voltage V_2 at the second coil directly relates to the current through the first coil I_1 using the mutual inductance M. When k equals 1, the coupling M is at a maximum. At k is 0, there is no coupling and no power can be transferred.
The term omega (ω) is the angular frequency at which the two-port operates and is also a factor for the induced voltage. At a higher frequency the change in the magnetic field is increased, from Faraday's law it follows that the induced voltage is increased.

3.1.2. Power transfer

In our wireless power transfer system the coils are placed relatively far apart, i.e. the coupling is low ($k \approx 0.1$). However, the power transfer should still be more than 5 watts. As seen in the section above, the coupling between the coils and the angular frequency are both directly related to the induced voltage. The induced voltage powers the load. Thus, to increase power transfer the angular frequency and the coupling need to be maximized within the bounds of our system.

Firstly, the theoretical power transfer possible over the airgap should be defined. Starting from Equation 3.3, the phasor currents and voltages are defined. The power transferred is the real part of the apparent power $\mathbf{S}$ through the system.

$$\mathbf{S} = \mathbf{V_1}\mathbf{I_1^*} \quad [\mathrm{W}] \tag{3.6}$$

$$P = \mathrm{Re}(\mathbf{V_1}\mathbf{I_1^*}) = -\mathrm{Re}(\mathbf{V_2}\mathbf{I_2^*}) \quad [\mathrm{W}] \tag{3.7}$$

This results in the real power defined as:

$$P = -\mathrm{Re}(j\omega M \cdot \mathbf{I_1} \cdot \mathbf{I_2^*}) \quad [\mathrm{W}] \tag{3.8}$$

For maximum positive power transfer, there should be no reactance, i.e. the phase of the apparent power should be 0°. The minus in Equation 3.8 for the receiving side (due to current convention of a two-port, see Figure 3.1) makes that the term $j\omega M \cdot \mathbf{I_1} \cdot \mathbf{I_2^*}$ should have a phase of 180°, in order to have this maximum positive power transfer.

The imaginary unit j adds a 90° shift to the multiplication of $\mathbf{I_1}$ and the complex conjugate $\mathbf{I_2^*}$, so the result of the multiplication should be 90°. $\mathbf{I_1}$ should lead $\mathbf{I_2}$ with 90° to get a 180° phase in the full term. For an arbitrary current angle, the power transfer can be represented by a sine function of α, where α is the angle between $\mathbf{I_2}$ and $\mathbf{I_1}$.

$$P = \omega M \cdot I_1 \cdot I_2 \cdot \sin\alpha \quad [\mathrm{W}] \tag{3.9}$$

I_1 and I_2 are the RMS values of the currents trough the coils L_1 and L_2 respectively. The mutual inductance M and angular frequency ω are defined as previously stated. The requirement for $\alpha = 90°$ is satisfied in Section 3.1.3 using capacitors. Let us assume for now that this requirement has been met.

The PoR states that the system should deliver 5 watts. The worst case within our specifications would be 70% efficiency at the load with 90% efficiency of the transmitter. Assumed is that the transferring coils are loss-less and all power is transferred according to Equation 3.9. The minimal efficiency of the receiver must be $70\%/90\% = 78\%$. The power that is delivered through the airgap is therefore $5/78\% \approx 6.4$ watts.

3.1.3. Tuning circuit

In the previous section, α was determined to be 90° for maximum power transfer, with all other factors constant. To achieve this, the phase of $\mathbf{I_2}$ needs to lag $\mathbf{I_1}$ with 90°. To change the phase of $\mathbf{I_2}$ an impedance is required. The following constraint is added to Equation 3.3 for shifting the phase:

$$\mathbf{V_2} = Z_t \cdot -\mathbf{I_2} \quad [\mathrm{V}] \tag{3.10}$$

The minus is due to the current defined as going in the two-port. To deliver positive power, the current must be negative. Z_t is defined as $Z_t = R + X_t$, where Z_t is the total additive impedance, R is the equivalent series resistance (Section 3.2) and X_t is the added tuning reactance. Adding Equation 3.10 to Equation 3.3 results in the following formula for the relationship between $\mathbf{I_1}$ and $\mathbf{I_2}$:

$$\mathbf{I_2} = \frac{j\omega M}{-Z_t - j\omega L_2} \cdot \mathbf{I_1} \quad [\mathrm{V}] \tag{3.11}$$

For $\mathbf{I_2}$ to be 90° lagging, the reactance in the denominator must be cancelled. The term $j\omega M$ in combination with $(-1) \cdot R$ will exactly shift the phase by 90°. This leaves us with the following constraint:

$$X_t = -j\omega L_2 \tag{3.12}$$

Let us use a capacitance for X_t to try to satisfy this formula.

$$\frac{1}{j\omega C_2} = -j\omega L_2 \tag{3.13}$$

This leaves the constraint:

$$\omega_0 = \frac{1}{\sqrt{L_2 C_2}} \quad [\mathrm{rad}] \tag{3.14}$$

This constraint is the same formula as for a resonant LC-circuit. The tuning capacitor C_2 must be chosen in such a way that the system is in resonance at the desired frequency. This will achieve maximum theoretical power transfer.

In a similar manner the input sees a reactance of the coil it powers, as can be seen in Equation 3.15. For the input we can also simply compensate this reactance L_1 with a capacitor C_1. The constraint of Equation 3.14 must hold for the input as well, so the frequency must be the same.

$$\mathbf{V_1} = \left(\frac{(\omega M)^2}{R} + j\omega L_1\right) \cdot \mathbf{I_1} \quad [\mathrm{V}] \tag{3.15}$$

3.2. Tuned resonant circuit design considerations

The equivalent circuit can be extended with the tuning capacitors mentioned above. Considering real components are used, equivalent resistances are added as well. The equivalent series resistances (ESR) are the modelled losses of the wire or dielectric used. Figure 3.2 shows the tuned theoretical wireless power transfer system.

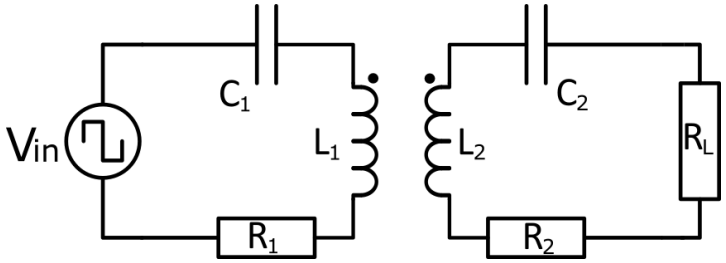

Figure 3.2: Wireless power transfer circuit with tuning capacitors and the equivalent series resistances R_1 and R_2

The equivalent resistances are the only sources of losses in the equivalent tuned circuit. The transferred power in the equivalent circuit is given by Equation 3.9 with $\alpha = 90°$. The total losses at the transmitter and receiver can be captured in the following formulas:

$$P_{in} = P + I_1^2 R_1 \quad [\text{W}] \tag{3.16}$$

$$P_{out} = P - I_2^2 R_2 \quad [\text{W}] \tag{3.17}$$

$$\eta = P_{out}/P_{in} \cdot 100\% \tag{3.18}$$

The resistive losses stem from the equivalent series resistances of the coil and capacitor. To minimize losses and increase efficiency high quality components must be used. The two subsections will elaborate on the choices made for the coil and the capacitor.

3.2.1. Coil Design Considerations

Two important factors in the coil design are the coil inductance and the coil AC resistance. These two parameters are related by the quality factor (Q-factor) as stated in Equation 3.19.

$$Q = \frac{\omega \cdot L}{R} \tag{3.19}$$

A bigger coil with a higher inductance is able to generate a stronger magnetic field, increasing mutual inductance. Thus a high inductance is desired. Also, a low resistance is desired as this will ensure that less power is lost when current flows through the coil. Therefore, the coil must have a high Q-factor.

As assembling a coil requires very precise engineering, due to the possibility of gaps between the windings and pitch variation, it was decided to buy the coils from an external company. There are multiple options available, but it was found that only the coils of 'Würth Electronics' had an extensive amount of data in the datasheets, where mainly the Q-factor as a function of the frequency applied was very useful. Figure 3.3 shows this relationship.

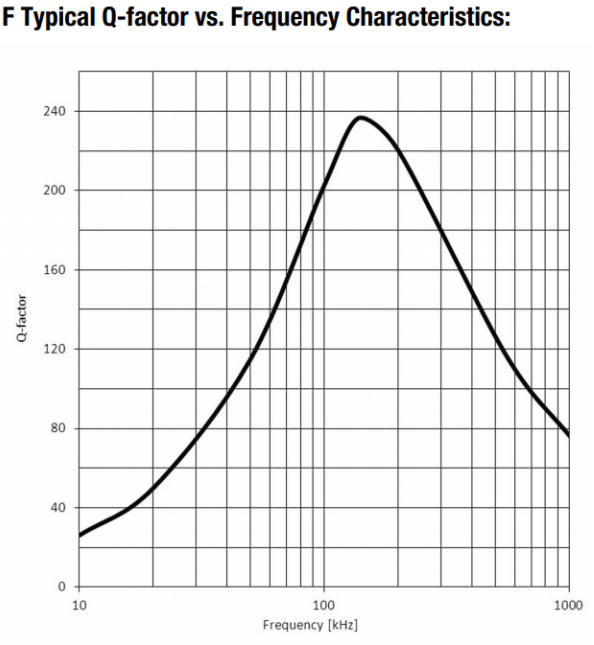

Figure 3.3: Q-factor as a function of the frequency applied [29]

This relationship is caused by two phenomena. The incline in Q-factor as the frequency rises (to 100 kHz) is caused by the linear relationship between Q and ω. The decline in Q-factor as the frequency rises (from 200 kHz) is caused by the skin effect in the Litz wire, which increases the AC resistance. As Q and R are inversely proportional, the Q-factor will decrease as this skin effect begins to play a role.

Skin Effect

In conductors, the penetration of high frequency signals is governed by the skin effect. This penetration is weaker within the conducting wire, thus the resistance in the inner part of the wire is larger, that that of the outer part of the wire. The depth at which the penetration of the signal is significant is called the skin depth (δ) and is among other things dependent on the frequency. As the frequency rises, the skin depth is smaller, thus the total resistance of a piece of wire increases, as Equation 3.20 shows. [30]

$$R/R_{DC} = \frac{\pi \cdot r^2}{\pi \cdot (2 \cdot r - \delta) \cdot \delta} \quad \text{with} \quad \delta = \sqrt{\frac{2 \cdot \rho}{\omega \cdot \mu}} \quad [\text{m}] \quad \text{and } r > \delta \tag{3.20}$$

In this approximation r is the radius of the wire, ρ is the resistivity , ω is the angular frequency and μ is the permeability. This skin effect phenomena is why, for high frequency coils, Litz wire is used. This Litz wire has lots of small strands of wire instead of one solid wire. These smaller strands have a much larger surface area relative to their size and will thus have a lower resistance at high frequencies compared to normal wire. This is shown in Figure 3.4.

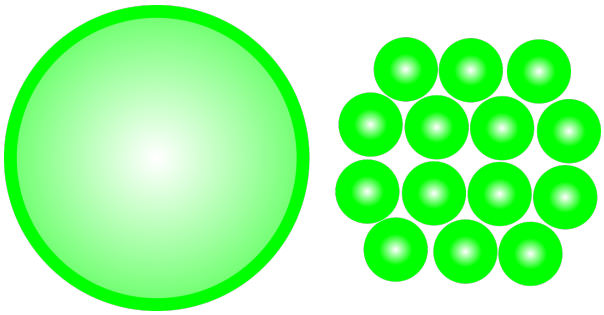

Figure 3.4: Illustration of the skin effect in Litz Wire. Green shows a low AC resistance

However, also in Litz Wire skin effect plays a role. This is seen in Figure 3.3. For example, for a copper wire with a radius of $0.2mm$ this phenomena starts to effect the resistance around 150 kHz. This is shown in Figure 3.5

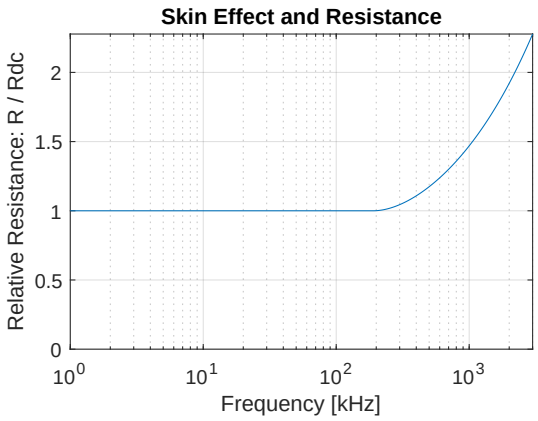

Figure 3.5: The resistance in Litz wire

A number of coils were considered, with the coil inductance and Q-factor in mind. The highest inductance and Q-factor within the size limitations was found in coil '760308110' from 'Würth Electronics'. [29]

3.2.2. Capacitor Design Considerations

As efficiency is an important requirement, this also has to be considered when choosing one or multiple tuning capacitors. Ceramic capacitors will be used, because these can withstand both positive and negative voltages as opposed to electrolytic capacitors. The three most common type of dielectric material in ceramic capacitors are X7R, Z5U and NP0. These names are the industry standards for referring to the materials and manufacturing. The difference in equivalent series resistance (ESR) between these three materials is significant. The dissipation factor (DF) is a measure for the losses in a capacitor. The dissipation factor of X7R and Z5U capacitors are generally above 1.5%, while NP0 capacitors generally have a dissipation factor below 0.1%. This is directly related to the ESR as seen in Equation 3.21. Incidentally, for NP0 materials the dielectric constant remains constant up to about 1 GHz. Thus NP0-type dielectric ceramic capacitors with the correct size are used. [31]

$$ESR = \frac{DF}{\omega \cdot C} \quad [\Omega] \tag{3.21}$$

3.2.3. Equivalent circuit resistances

The real coils and capacitors have been chosen in the sections above. The ESR of the real components can be calculated. For these calculations, the frequency of 150 kHz is assumed. The choice for this frequency is stated in Section 3.7.

For a frequency of 150 kHz the Q-factor of the coils is 235. The coils an inductance of 24 μH. The capacitors have a dissipation factor of 0.1%. With the frequency set, the constraint described by Equation 3.14 can be used to set the size of the capacitor. At 150 kHz the capacitor size is 46.9 nF. Using the Equation 3.19 and 3.21 the real resistances are calculated:

$$R_{coil} = \frac{\omega \cdot L}{Q} = \frac{150 \cdot 10^3 \cdot 2\pi \cdot 24 \cdot 10^{-6}}{235} = 96 \quad [\mathrm{m}\Omega] \tag{3.22}$$

$$R_{capacitor} = \frac{DF}{\omega \cdot C} = \frac{0.001}{150 \cdot 10^3 \cdot 2\pi \cdot 46.8 \cdot 10^{-9}} = 22 \quad [\mathrm{m}\Omega] \tag{3.23}$$

3.3. Functional block diagram

The transmitter is responsible for powering the coil L_1 to create a magnetic field to transfer power. As stated in the previous section, the maximum power transfer is achieved when the receiver is powered in resonance. The additional task of the transmitter is creating the right frequency to power the transmitter coil.
The design consists of an oscillator, capable of generating the oscillating signal for the transmitter. An inverting circuit is responsible for connecting the load to the resonant circuit. This inverter is powered by a gate-driver that uses the signal of the oscillator to switch correctly. A functional block diagram of the transmitter is given in Figure 3.6.

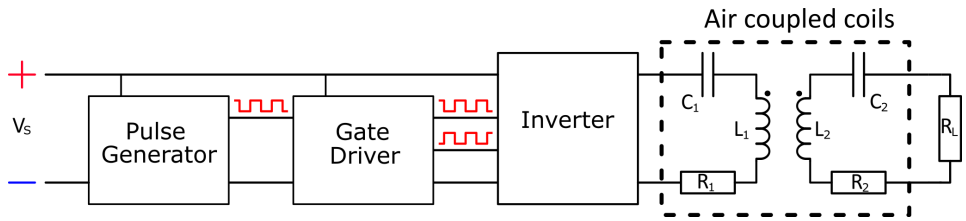

Figure 3.6: The functional block diagram of the transmitter

3.4. Oscillator

The oscillator needs to generate an oscillating signal. As the LC-circuit must be powered with a high enough frequency to transfer enough power, our oscillator must be well within our operating range. In the PoR the range for operation is defined between 80 kHz and 300 kHz. Therefore the oscillator must be able to generate at least a frequency of 300 kHz and the oscillation frequency must be tuneable. The tuning is needed to precisely set the frequency to the resonant frequency of the LC-circuit. Properly tuning the circuit will improve the efficiency immensely. In short, the oscillator must be able to satisfy the constraints given in Section 2.2.

The LTC6992-1 [32] meets the above mentioned specifications. The oscillation frequency can be up to 1 MHz. The oscillation is set using a resistor. A schematic of the inner workings can be seen in Figure 3.7.

At pin 3 the R_{SET} is connected. A control circuit using a comparator keeps the voltage at 1 V over the resistor. The current through the resistor determines the oscillation frequency. The higher the resistance, the lower the oscillation. The oscillation is fed to a divider, which will not be used. On pin 1 V_{MOD} is given. This is set to roughly 0.5 volt. The voltage determines the duty cycle of the oscillator and a 50% duty cycle is needed. Lowering the duty cycle will input less power into the system, but for most cases the power in the LC-circuit should be maximum. The output is a square wave with 50% duty cycle at our desired frequency.

The losses in the LTC6992-1 are low. The current consumption at 5 volts is around 130 μA. The power consumption is 0.65 milliwatts. This low power consumption is very well suited for the low power system.

The LTC6992-1 needs to be powered with a 5 volt supply. Since the source is not fixed, a voltage regulator is needed. The MCP1702 [33] is a voltage regulator with high efficiency ($2.5\mu A$ used by regulator). For this reason the regulator was chosen.

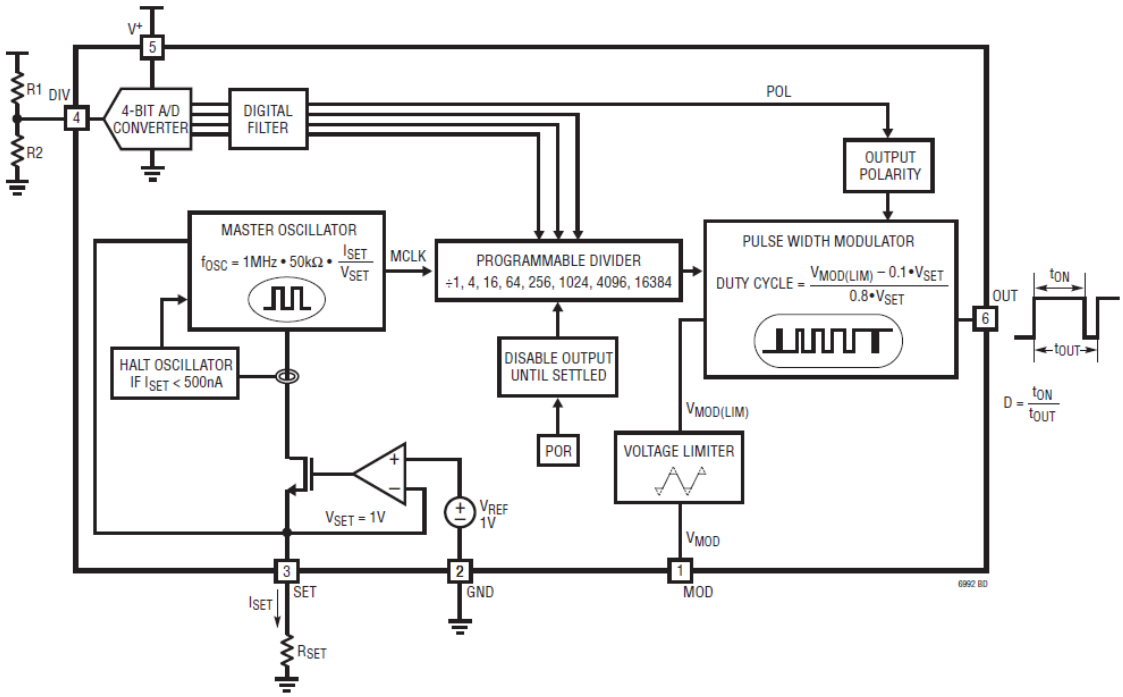

Figure 3.7: Functional block diagram of the LTC6992CS6-1 oscillator

3.5. Gate-driver

The oscillator does not have enough output power to drive the gates of the MOSFETs. Furthermore, proper control of dead-time is needed to eliminate the possibility of shoot-through currents. As will be determined in Subsection 3.6, the topology is a half-bridge configuration. To power the half bridge two gate-drivers are needed, a high-side driver and a low-side driver. The drivers must be able to operate at the resonant frequency of the LC-circuit. This gives one fast switching times while still being able to deliver the power needed for the gates. The high-side driver must also be able to create a voltage well above the source voltage of the source of the high-side MOSFET, thus high enough to properly turn on the MOSFET.

3.5.1. Bootstrap circuit

To achieve a high enough voltage a bootstrap circuit is used. This circuits drives the gate voltage above the output voltage (and thus above the source voltage of the high-side MOSFET) and ensures that the MOSFET is turned on properly. This is done using a diode and a capacitor. The schematic (without diode voltage drop) is given in Figure 3.8. The capacitor is connected to the floating source of the high-side MOSFET. When the low-side MOSFET is turned on this node is connected to ground. The capacitor is charged to (almost) the supply voltage through the diode. When the high-side is switched the source node becomes floating. The capacitor cannot discharge through the diode and the voltage over the capacitor stays the same. The floating side lifts the total voltage over the capacitor to ground to above the supply voltage. The gate-source voltage is high enough to get the MOSFET fully on. Using the bootstrap circuit both MOSFETs turn on similarly and properly (saturation mode), decreasing possible resistance that they may cause.

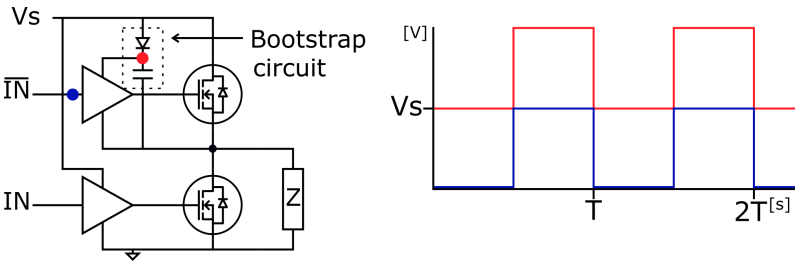

Figure 3.8: Bootstrap circuit used for driving a high-side MOSFET

3.5.2. Dead-time

The second objective of the gate-driver is control over the dead-time. When both MOSFETs are on, the resistance between the supply voltage and ground is very low. This causes a high current that could possibly destroy the MOSFETs. Furthermore, all this energy is lost. To account for this, a dead-time is used. This means that the control signal is adjusted in such a way that the high-side turn-on is a little later than the low-side turn-off and vice versa. This has been visualized in Figure 3.9. A drawback of implementing dead-time is that the load will see an open terminal for a short period of time. This disrupts the oscillation and introduces harmonics. These harmonics will translate into losses and that is undesirable. To minimize these losses, the dead-time should be as short as possible, meaning that the other side must turn on exactly when one side is closed. A tunable dead-time is therefore desirable.

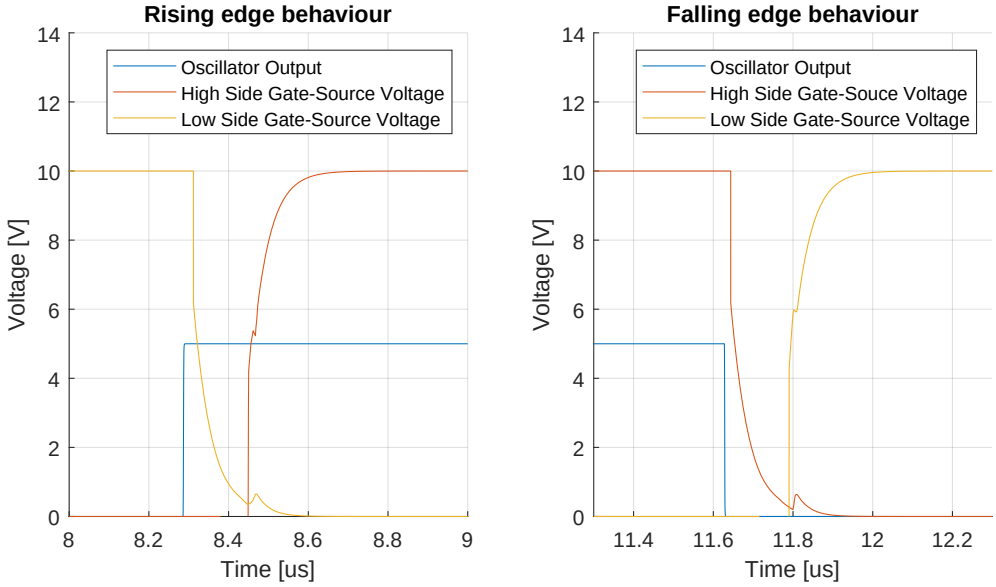

Figure 3.9: Simulation of the 200 ns dead-time in the inverter

3.5.3. LM5104

The LM5104 [34] meets the above mentioned specifications. The LM5104 is an integrated high-side and low-side driver. The chip has a built in dead-time control, with a resistor to tune the dead-time. It only requires a single input, as it internally inverts the signal. An internal bootstrap diode is included, but an optional fast recovery bootstrap diode can be placed in parallel to decrease losses.

The main choice of the LM5104 over other drivers is first of all that an internal inverter is included. This eliminates the need to add an extra component that does this. Furthermore, both the high-side and low-side drivers are included in one package. This makes it easier to assemble but also allows the chip to control the dead-time accurately. With distinct drivers further effects such as inductive loops and parasitic capacitance are harder to eliminate.

A drawback is that the losses due to control will be concentrated on and around the driver package. The package could heat up significantly. The charging and discharging of the gates of the MOSFETs

pass through the driver and cause dissipation as can be seen in Figure 3.10a. Further losses are found in the bootstrap diode as can be seen in Figure 3.10b.

The capacitance of the MOSFETs together will be 6600 pF. The specs of the MOSFETs are discussed in Subsection 3.6.2. From the figure the power dissipation comes down to 1.5 times the power dissipated at $C_L = 4400$ pF as our capacitance is 1.5 times higher. This leaves one with a total estimated power consumption of around 435 milliwatt. This is a significant power loss at a 5 watt load, but these losses are unavoidable, as this is the energy required for turning on and of the inverter. Alternatives would have similar losses.

The LM5104 requires a 8 V to 14 V supply to operate. To be sure not to exceed these limits, a voltage regulator will power the LM5104. The voltage regulator used is the TL750L10 [35]. This regulator is a low dropout voltage (330 mV) regulator with high efficiency power delivery. The efficiency is high (1 mA average used by regulator) and it can deliver $10V$, thus it fits the requirements.

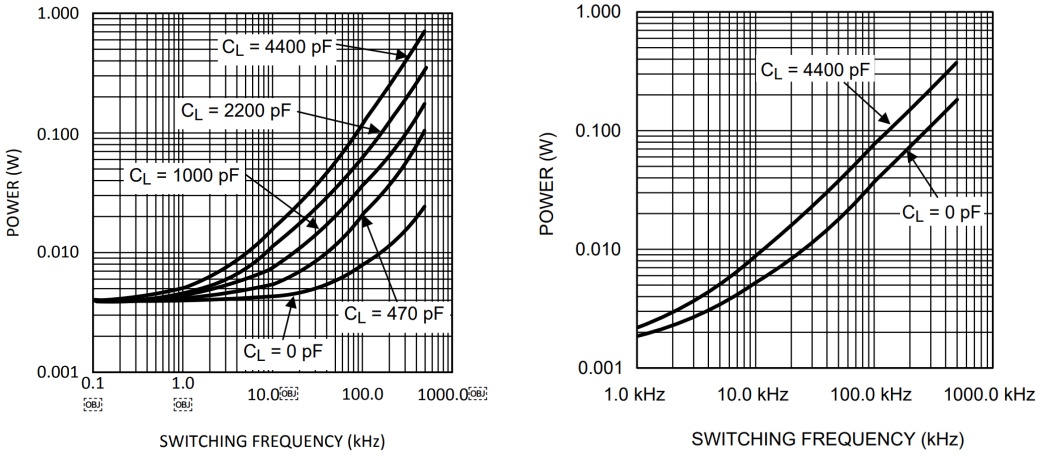

(a) Losses in gate-driver due to gate charge (without diode losses)

(b) Losses in gate-driver due to bootstrap diode losses

Figure 3.10: Losses in the gate-driver for different frequencies

3.6. Inverter Circuit

A typical inverter transforms a DC voltage into an AC voltage. This is done by switching the voltage from positive to negative on the terminals of the output. Modern inverters achieve this by using MOSFETs, an electrical switch that can be controlled using an electric signal. Due to the need to control the frequency over the coil and having a high operating frequency, as stated in the PoR, using MOSFETs is an obvious choice. In Subsection 3.6.2 the design choices concerning the MOSFETs are described in detail.

3.6.1. Topology

Multiple topologies of MOSFETs will achieve the goal of an AC at the output. The output of the inverter, the resonant circuit, determines mainly what types of topologies are useful. As shown in Subsection 3.6.3, only the resonant peak draws significant power. Therefore, the inverter topology must be chosen such that it powers the resonant circuit at its resonance frequency. Doing otherwise would only increase losses, which is undesirable.

Two widely used topologies are considered. The full-bridge inverter, and the half-bridge inverter. These topologies can power the resonant circuit at resonance and these simple topologies do not require complex control to achieve this. Figure 3.11 shows the topologies and their switching modes.

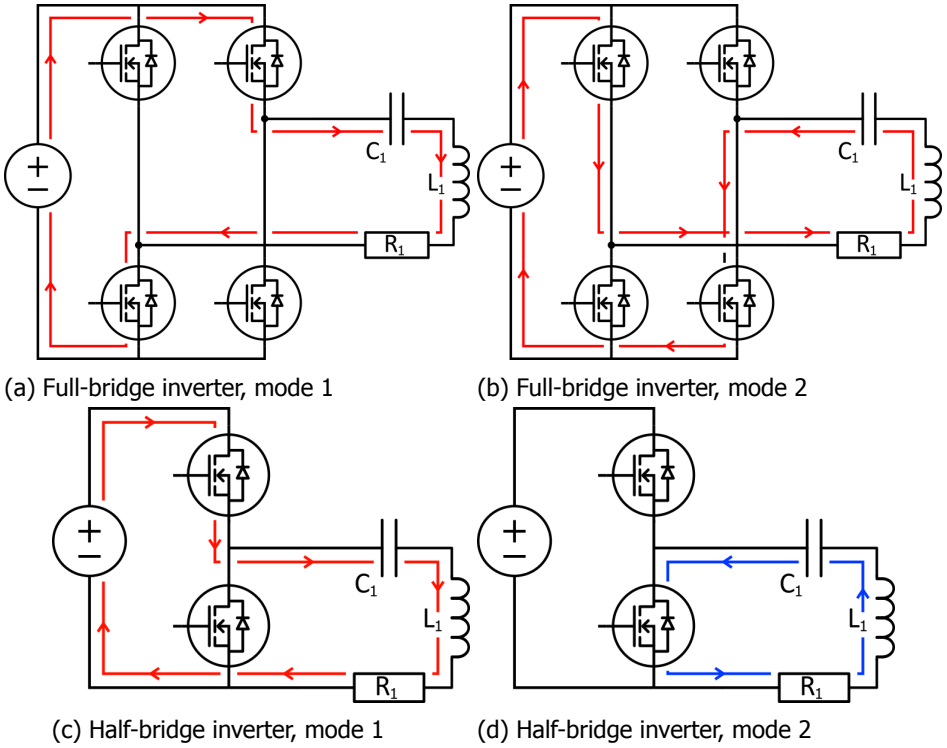

(a) Full-bridge inverter, mode 1 (b) Full-bridge inverter, mode 2

(c) Half-bridge inverter, mode 1 (d) Half-bridge inverter, mode 2

Figure 3.11: Full-bridge and half-bridge inverter topologies

The two topologies work differently in creating an inverting signal. The full-bridge inverter inverts the signal fully, by reversing the poles at a fixed frequency. This is shown in Figure 3.11a and 3.11b. The red color indicates that the system is powered by the source.
The half-bridge inverter uses the resonance of the LC-circuit to have an inverting signal. Similarly to pushing a swing, the half-bridge inverter excites the resonant circuit in phase to add energy to the system. With each cycle the inverter keeps adding energy, continually keeping the system in resonance. Figure 3.11c and 3.11d show this cycle. The blue color indicates that the system is oscillating on itself.

Source voltage

For the half-bridge inverter to deliver the same power to the resonant circuit, it must operate at twice the voltage. The full-bridge output voltage will have a maximum amplitude of double that of the source voltage. Considering that both half-bridge and full-bridge oscillation circuits will reach a steady state, they will have the same impedance. For the source to deliver the same power in both cases the voltage over this impedance must be the same.

To achieve the same voltage, the filtering of the oscillation circuit must be taken into account. As Subsection 3.6.3 describes, the resonant circuit acts as a filter. Considering the voltage switches from maximum to zero, one can conclude that a DC offset is included at half the supply voltage. With the filter of the LC-circuit, this DC offset is removed and the LC circuit is given an oscillation between $\pm$ half the supply voltage.

The requirement is to power a 5 watt load. The equivalent load seen by the source is a few tens of ohms (simplified to only resistive impedance as the system is in resonance). The power delivered to the load is given by $P = V^2/R$. V^2 will be in the order of 10^2 and V will be between 10 - 20 volts. Therefore, the voltage over the half-bridge inverter will not exceed what a normal power outlet could deliver. The PoR does not state a fixed voltage, so this voltage is chosen as desired by the receiver.

Damped oscillation

As can be seen in Figure 3.11d and as is mentioned above, the LC-circuit oscillates by itself for some time. The blue color indicates this. If the oscillation did not lose any energy, the oscillation would not

dampen, but the LC-circuit uses real components and wires and these have internal resistances. The oscillation is damped and loses energy consistently. The formula for a damped LC system (2nd order system) is given in Equation 3.24 and Figure 3.12 is an example of a waveform caused by a damped system.

$$\ddot{I}(t) + 2\zeta\omega_0\dot{I}(t) + \omega_0^2 I(t) = 0 \tag{3.24}$$

The undamped natural frequency is $\omega_0 = \frac{1}{\sqrt{LC}}$ and the damping ratio $\zeta = \frac{R}{2}\sqrt{\frac{C}{L}}$. R is the equivalent series resistance of all the wires, the capacitor and the coil in the oscillation circuit. The damped frequency is given in Equation 3.25.

$$\omega_d = \omega_0\sqrt{1-\zeta^2} \quad \text{[rad]} \tag{3.25}$$

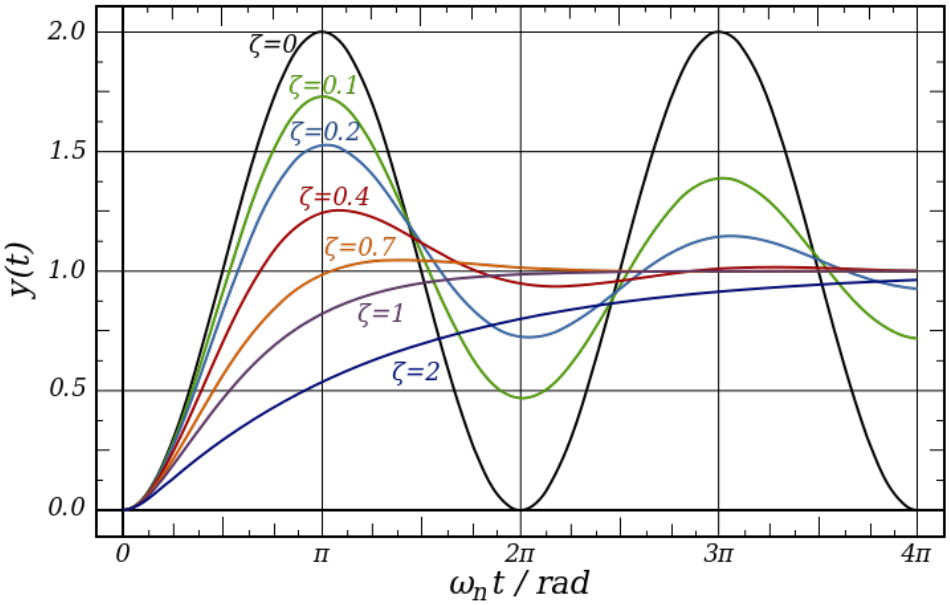

Figure 3.12: An exaple of a damped wave with different damping ratios

With our oscillating circuit the equivalent series resistance adds up as follows. $R = ESR_C + ESR_L + R_{wire} + R_{MOSFET}$. The exact combined value for the wire and MOSFET resistances is unknown but is estimated to be around a few tens of milliohms. Using the ESR of the coil given in Section 3.2.1 and the ESR of the capacitor given in Section 3.2.2 the total resistance (in milliohm) adds up to $R = 22 + 96 + 30 = 148m\Omega$ (Equation 3.22 and 3.23). The 30 milliohm is an estimation of the extra resistance added by the wires and MOSFET combined.

The following frequency follows from accounting for the resistance: the damping ratio ζ is given above. filling in the values for R, L and C gives us a damping factor of 0.0026. The damped frequency is given by Equation 3.25. The damped frequency will be changed by a factor of $\sqrt{1-\zeta^2}$ and this value is 0.99999, which is very close to 1. Realistically, the damping does not have effect on the frequency.

Resistive losses

The resistive losses in the MOSFETs differ for the two topologies, regardless of what MOSFETs are used. For the full bridge configuration the current delivered by the source to the resonant circuit also passes through two MOSFETs, in the half-bridge case it is only one MOSFET. This can clearly be seen in Figure 3.11. The current drawn is equal for both resonant circuits, because the LC-circuits are equal and they draw the same amount of power. Therefore, the resistive losses trough the MOSFETs are twice as high in the full bridge configuration.
Furthermore, less drivers are required for the half bridge inverter and losses could further be reduced. From an efficiency perspective, the half bridge topology would outperform the full-bridge configuration

in terms of resistive losses.

Weighing up all the benefits and shortcomings of the half-bridge and full-bridge inverter and considering our demands stated in the PoR, the choice for the inverter topology will be a half-bridge inverter. The half-bridge inverter has lower losses than the full-bridge inverter. The source voltage is not fixed and is not a constraint. Less control circuitry is required for the half bridge inverter.

3.6.2. MOSFETs

As made clear by the previous section, the MOSFETs could potentially have a huge impact on the efficiency of the system. To prevent this, high quality, low loss MOSFETs must be chosen. In this section the parameters concerning the MOSFETs are elaborated upon and a MOSFET for the inverter is chosen.

Doping type

First of all the doping type is discussed. MOSFETs can both be n-type and p-type. The type refers to the channel and the doping applied. An n-type MOSFET has positively doped silicium as the channel. The drain and source are negatively doped. The opposite is true for a p-type MOSFET. For the channel to conduct, the n-type needs a positive gate-to-source voltage (V_{gs}) and the p-type needs a negative voltage.

Using both n-type and p-type may be desirable, because one could use the same signal to both MOSFETs and they would switch alternately. Furthermore, if a p-type MOSFET was used, the high-side MOSFET would not need a complex driver to boost the gate voltage high enough to properly turn on the MOSFET. A negative voltage could simply be applied.

There are some mayor drawbacks to using p-type MOSFETs however. Firstly, the doping makes it so that so-called 'holes' must move through the substrate to create the channel for conduction. Comparing with the n-type the electrons move to create the channel. The 'holes' have a worse mobility than the electrons (about 1/3 of the mobility in silicon [36]), meaning that more effort is required to reach the desired functionality, or to fully turn on. Practically, this means that the switching times are worse and/or the on-resistance is higher.
Using both types in the half-bridge inverter with different switching times could cause both MOSFETs to be on for a certain amount of time. The source could short and the high current destroys the MOSFETs. This could be prevented by creating a dead time, in which both MOSFETs are off. But that would require more control and add distortion to the resonating circuit and result in losses.

In conclusion, the n-type MOSFETs best suite the design.

Criteria

With the type of MOSFET determined, a specific MOSFET must be chosen. Several high-end MOSFETs are listed in Table 3.1. The MOSFETs have been selected from the Farnell (nl.farnell.com) website. Most MOSFETs in the table operate in the range of 40-80 V. This is well within our needs and not too high to effect the characteristics which are most important: the on resistance ($R_{ds(on)}$) and the gate charge (Q_g).

$R_{ds(on)}$ is the resistance that the MOSFETs inhibit when in saturation mode. The RMS current trough the MOSFETs in the inverter is around 1.3 amperes. The power dissipation due to the resistive losses lie within the range of 8.5 milliwatts to 37 milliwatts.

As is mentioned in Section 3.5 the charging and discharging of the MOSFETs causes losses in the gate-driver. To minimize losses on this front, the gate charge needs to be as minimal as possible. Precisely describing the losses for each MOSFET and accompanying driver is hard, but a simple formula exist to quantify the gate losses.

$$P_{gate} = Q_g \cdot V_{gs} \cdot f \quad [\text{W}] \tag{3.26}$$

Table 3.1: MOSFETs considered for the inverter

Mosfet	$R_{ds(on)}$ $[m\Omega]$	V_{ds} $[V]$	I_{ds} $[A]$	$V_{gs(th)}$ $[V]$	Q_g $[nF]$	t_{on} $[ns]$	t_{off} $[ns]$	t_{rise} $[ns]$	t_{fall} $[ns]$	P_{loss} $[mW]$
STD30NF06LT4	22	60	35	2.5	23	30	65	105	25	54.4
BUK964R-40E	3.4	40	75	2.1	52.1	34	88	64	60	38.6
NTMS5838NL	20	40	5.8	3.0	17	11	17	23	4	49.1
NTMS5835NL	10	40	9.2	3.0	40	15	22	45	9	52.9
IRF7842PBF	5	40	18	2.25	33	14	21	12	5	30.7
PSMN017-80PS	15.2	80	50	4	22	14	27	12	8	52.1
IPD70N10S3L-12	11.5	100	70	2.4	59	12	35	6	7	61.9
STD36P4LLF6	20.5	400	36	2.5	22	43	148	47	19	51.1

Using the two most important characteristics, a ranking can be determined to choose the best MOSFET. The result of the power dissipation can be seen in the last column of Table 3.1. The best MOSFET is the IRF7842 [37]. This MOSFET will be used in the inverter.

$$P_{loss} = P_{gate} + I^2 \cdot R_{ds(on)} \quad [\text{W}] \tag{3.27}$$

3.6.3. Harmonics

The inverter has a square wave, these contain a lot of higher order frequencies, harmonics. When Equation 3.14 is satisfied, the LC resonant circuit is in resonance. Other frequencies supplied to this circuit will be damped heavily with respect to the resonant frequency. This can be seen in Figure 3.13b. Having this filter applied means that this resonant circuit can be fed with a square wave oscillating at the resonant frequency. The harmonics of this square wave that are at 3, 5, 7, etc. times the base frequency will not be amplified, while the resonant frequency will be amplified significantly.

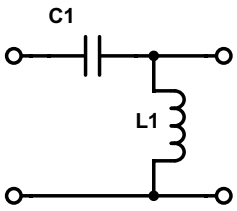

(a) LC resonant circuit two-port diagram

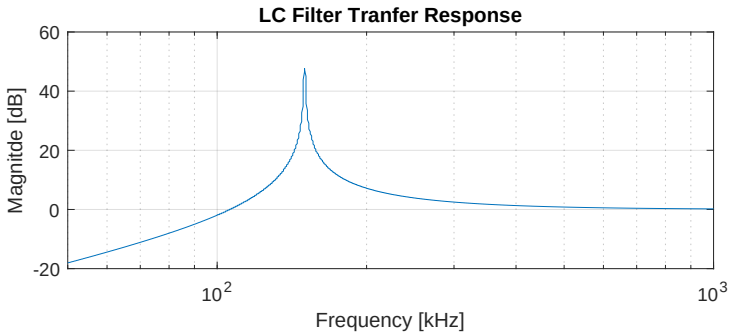

(b) Transfer function of the LC resonant circuit

Figure 3.13: The LC resonant circuit

3.7. Operating Frequency Optimization

There are several different frequency dependent elements in the design that make for a frequency dependent power loss and thus a frequency dependent efficiency. These are the amount of power that is transferred, the resistance of the coil and tuning capacitor and the losses in the control circuit. Therefore, an analysis has been done to optimize the operating frequency.

3.7.1. Power Transfer Influences

Firstly, the effect of the frequency on the the transferred power in the circuit is discussed. The relationship between the power transferred and the frequency is described in Equation 3.28, where α is the phase angle between I_1 and I_2, which should be 90° (Section 3.1.2) [12].

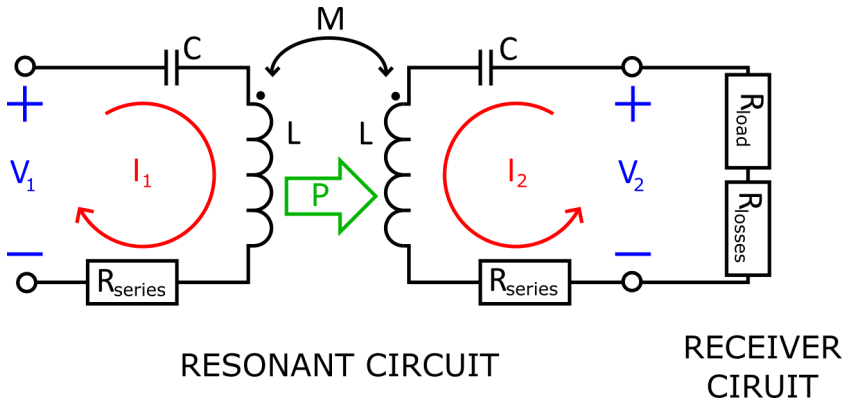

Figure 3.14: Power transfer in the resonant circuit

$$P = \omega \cdot M \cdot I_1 \cdot I_2 \cdot sin(\alpha) \quad [\text{W}] \tag{3.28}$$

Important to notice are the currents through the resonant circuits as these are related to the power lost in the equivalent series resistances of the components. In order to determine these losses, the currents through the components have to be known. The ratio between the current in the transmitter coil and the receiver coil is given in Equation 3.29. This has been derived from Equation 3.11 when Equation 3.14 holds.

$$|\mathbf{I_2}| = \frac{\omega M}{R} \cdot |\mathbf{I_1}| \quad \Rightarrow \quad I_2 = \frac{\omega M}{R} \cdot I_1 \quad [\text{A}] \quad \text{with} \quad R = R_{load} + R_{losses} + R_{series} \quad [\Omega] \tag{3.29}$$

As the power consumed by the load is 5 W and the voltage over the load is 5 V, an RMS current of 1 A will flow. Assuming 6.4 W has to be delivered to the load (Section 3.1.2) and an RMS current of 1 A will flow, the equivalent resistance of the losses (R_{losses}) can be modeled as a 1.4 Ω series resistance. With this model, 6.4 W will be consumed by the receiver when delivering 5 W to the load. For now, an equivalent series resistance (R_{series}) in the resonant circuit of 100 mΩ is assumed.

With Equation 3.28 and Equation 3.29, a formula for the current through the transmitter resonant circuit can be obtained:

$$I_1 = \frac{P}{\omega M} \cdot \frac{1}{I_2} = \frac{P}{\omega M} \cdot \frac{R}{I_1 \cdot \omega M} = \frac{P \cdot R}{I_1 \cdot (\omega M)^2} \quad [\text{A}] \tag{3.30}$$

$$I_1^2 = \frac{P \cdot R}{(\omega M)^2} \quad \Rightarrow \quad I_1 = \frac{\sqrt{P \cdot R}}{\omega M} \quad [\text{A}] \tag{3.31}$$

Also, the current through the receiver can be obtained:

$$I_2 = \frac{\omega M}{R} \cdot I_1 = \frac{\omega M}{R} \cdot \frac{\sqrt{P \cdot R}}{\omega M} = \sqrt{\frac{P}{R}} \quad [\text{A}] \tag{3.32}$$

From this the power dissipated in the transmitter resonant circuit can be calculated:

$$P_{loss-1} = I_1^2 \cdot R_{series} = \frac{P \cdot R}{(\omega M)^2} \cdot R_{series} \quad [\text{W}] \tag{3.33}$$

$$P_{loss-2} = I_2^2 \cdot R_{series} = \frac{P}{R} \cdot R_{series} \quad [W] \tag{3.34}$$

$$P_{loss} = P_{loss-1} + P_{loss-2} = P \cdot (\frac{1}{R} + \frac{R}{(\omega M)^2}) \cdot R_{series} \quad [\text{W}] \tag{3.35}$$

This results in a power loss and efficiency as seen in Figure 3.15.

$$P_{load} = I_{rms}^2 \cdot R_{load} \quad \Rightarrow \quad I_{rms} = \sqrt{\frac{P_{load}}{R_{load}}} = \sqrt{\frac{5}{5}} = 1 \quad [\text{A}] \tag{3.36}$$

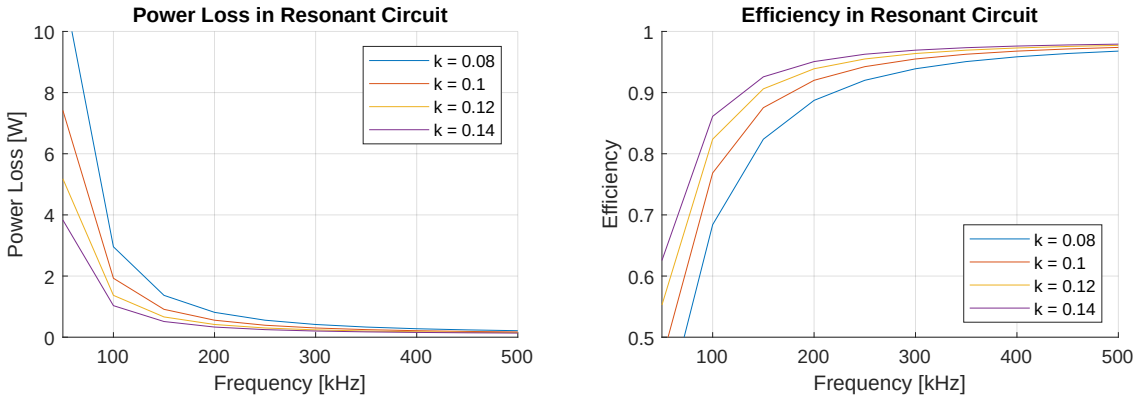

Figure 3.15: Power loss and efficiency of the resonant circuit (1)

Calculations with these formulas can be found in Section A.1.1 in Appendix A.1.

3.7.2. Coil Resistance Influences

Not only the amount of power transferred is dependent on the frequency, but increasing the frequency also leads to an increase in the resistance of the coils as described in Section 3.2.1. Finding an optimum between these two is the next step of the analysis. The series resistance of the resonant circuit can be derived from Equation 3.19 and Equation 3.21:

$$R_{series} = \frac{\omega \cdot L}{Q} + \frac{DF}{\omega \cdot C} \quad [\Omega] \tag{3.37}$$

Replacing the equivalent series resistance of Equation 3.35 will lead to the following equation:

$$P_{loss} = P_{loss-1} + P_{loss-2} = P \cdot \left(\frac{1}{R} + \frac{R}{(\omega M)^2}\right) \cdot \left(\frac{\omega \cdot L}{Q} + \frac{DF}{\omega \cdot C}\right) \quad [\text{W}] \tag{3.38}$$

L is the inductance of the coil used, the chosen coil has an inductance of $24\mu H$ [29]. Q is the quality factor of the coil used (Figure 3.3). DF is the dissipation factor of the tuning capacitor uses, which is 0.1% or 0.001. C is the capacitance of the tuning capacitor, which has been chosen to satisfy Equation 3.14 for different frequencies. This yields Figure 3.16 for the total power lost in the resonant circuit and its efficiency.

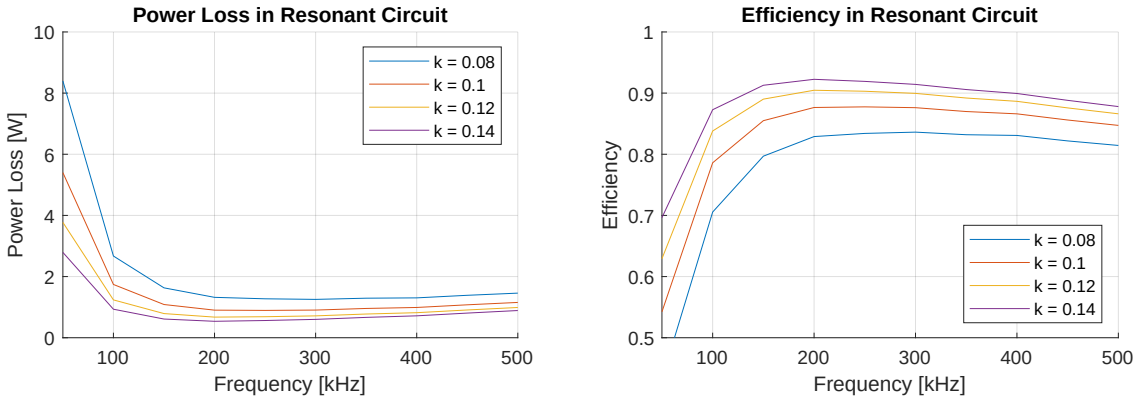

Figure 3.16: Power loss and efficiency of the resonant circuit (2)

Calculations with these formulas can be found in Section A.1.1 in Appendix A.1.

3.7.3. Control Circuit Influences

Not only the components of the resonant circuit , but also the gate-driver has a frequency dependent power loss (Figure 3.10). This power loss is added to the power loss inside the resonant circuit, to construct Figure 3.17.

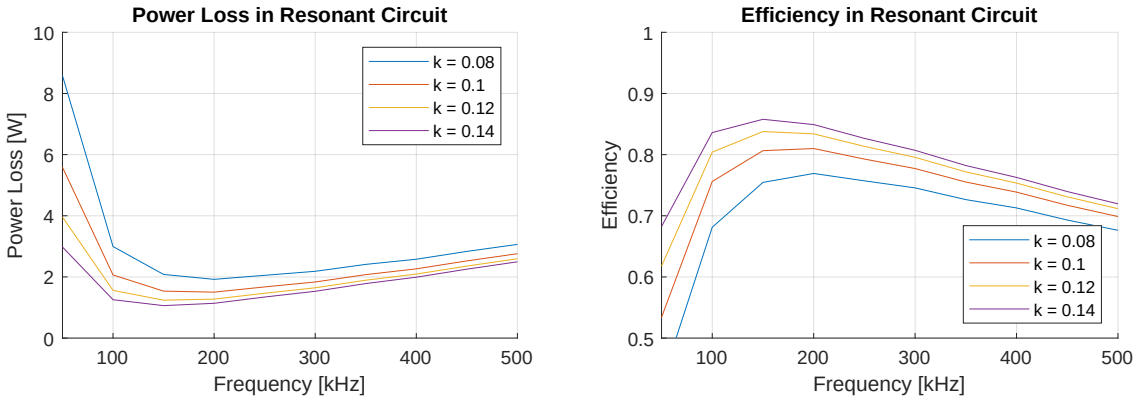

Figure 3.17: Power loss and efficiency of the resonant circuit (2)

Calculations with these formulas can be found in Section A.1.1 in Appendix A.1.

This figure shows that the highest efficiency for a coupling of $k \approx 0.1$ is reached with an oscillation frequency of 150 kHz. This will be the operating frequency of the system.

3.8. Final design

This section will discuss the final design. A clear block diagram of the full system is given. Simulations are included of this system to validate our design choices, within the context of the whole system.

3.8.1. Finalized design

The finalized design is shown in Figure 3.18. The final design consists of: A high frequency oscillator, to precisely set the frequency; The gate-driver, powering the MOSFETs with high speed, and preventing shoot-through; And the half bridge inverter with low-loss specifications. This all powers our resonant circuit to generate the desired magnetic field. Two voltage regulators are included to properly power the oscillator and the gate-driver.

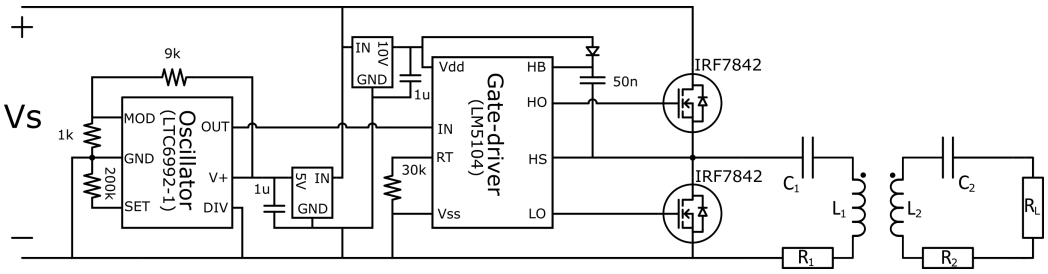

Figure 3.18: Full circuit schematic of the transmitter

To confirm the validity of the design, simulations are run demonstrating the desired functionality. The simulations give an indication of the efficiency of the system.

3.8.2. Simulations

The circuit has been simulated with the use of LTSpice. Some simulation results have been selected to best visualize the simulated workings. Figure 3.19 shows the control signals powering the inverter. The oscillator waveform and the accompanying gate-driver outputs.

Figure 3.20 shows how the resonant circuit is powered, the switching working of the inverter is visible in the half-bridge output and the oscillating working is seen in the oscillating current. With

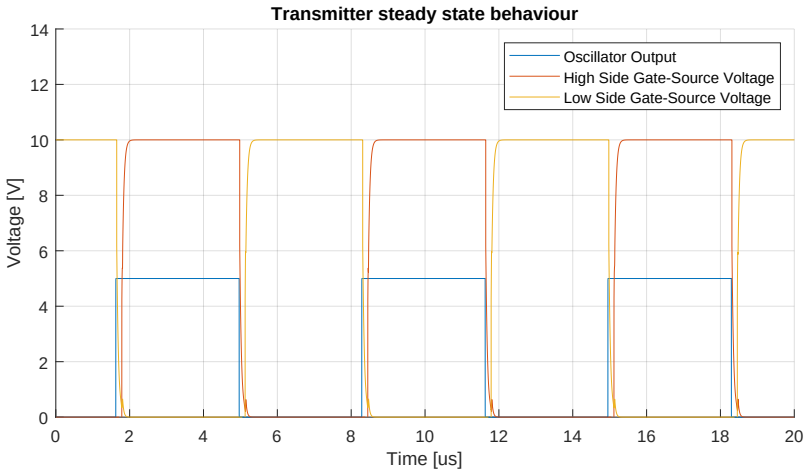

Figure 3.19: Oscillator and gate-driver simulation (1)

these waveforms the power can be calculated that goes into the oscillator. The multiplication of the voltage and current lead to an average half-bridge output power of 7.3 W. With the simulation, the output power of the equivalent circuit can be measured and the load power is estimated to be 6.4 W (The load being the full rectifier circuit and load). Thus from the simulations, it can be seen that the transfer efficiency over the airgap is 87.6%.

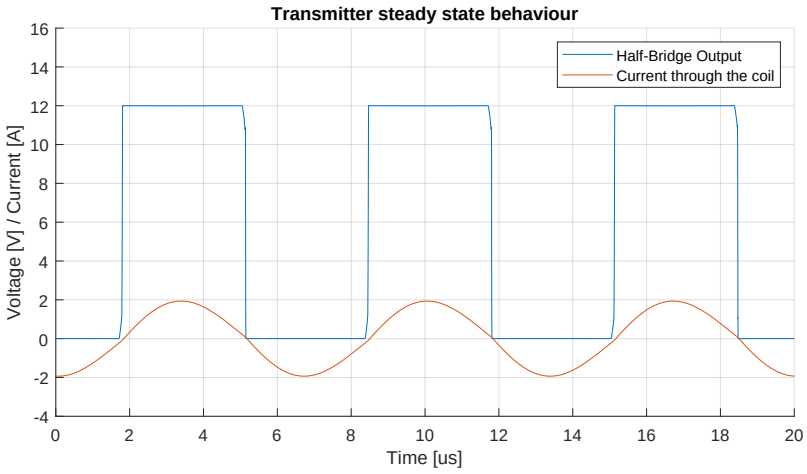

Figure 3.20: Resonant circuit simulation

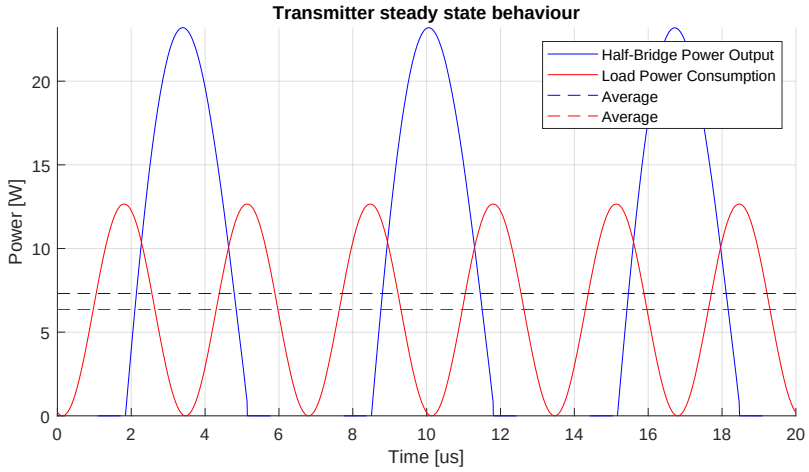

Figure 3.21: Resonant circuit input and output power

4

Results and Discussion

The results from the prototype are discussed. They are validated against the simulations and the final efficiencies are stated. The shortcomings and possible improvements and surprising results are listed in the discussion. Possible flaws in the initial design are addressed as well. In Figure 4.1 a picture of the transmitter can be seen.

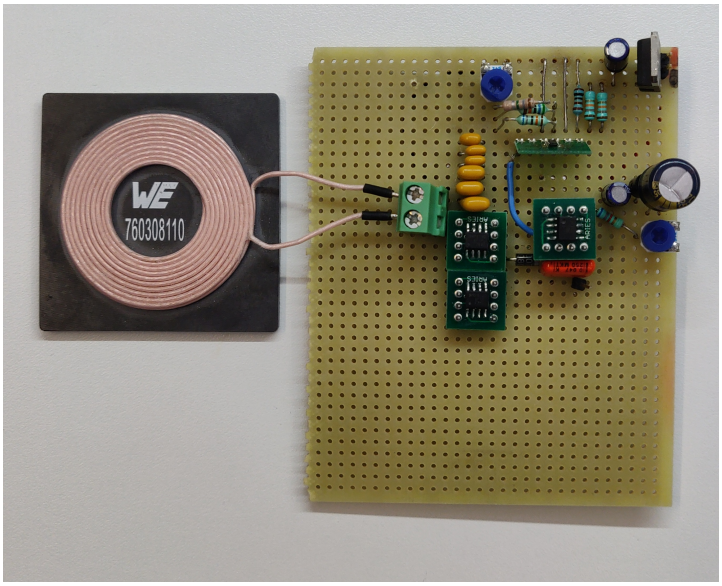

Figure 4.1: Picture of the transmitter prototype

4.1. Measurements

4.1.1. Methodology

The measurements are done of all relevant signals to verify the workings and to calculate the efficiencies. The waveform measurements are obtained using the TDS2022C oscillator waveform export function. Different points in the circuit were measured with a probe as seen in Figure 4.2: the oscillator output (1), the bootstrap output (2), the high-side gate signal (3), the low-side gate signal (4), the inverter output or resonant circuit input (5), the tuning capacitor voltages (6 & 7) and the resonant circuit output (8). Also the load output voltage was measured with a multimeter. All measurements were recorded separately, but are all aligned in time. This was done by setting the trigger on one channel of the oscilloscope which was connected at all times.

These exported waveforms are plotted using Matlab. The waveform data allows one to do computations as well, such as current and power derivation, and take time variant behaviour into account. Figure 4.3 shows the setup in which the measurements were taken.

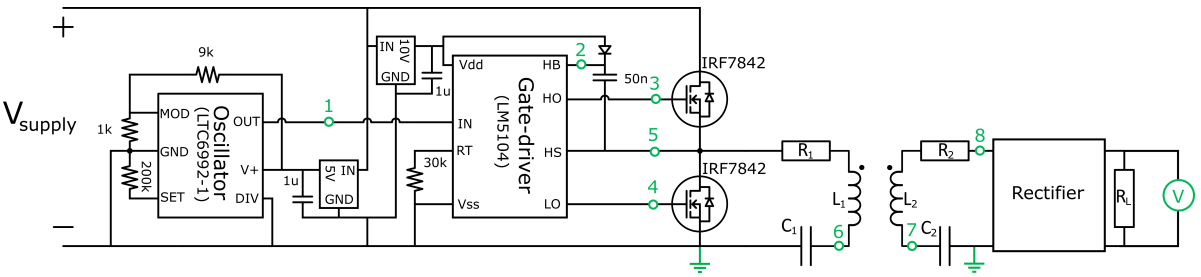

Figure 4.2: Measurement points in the circuit

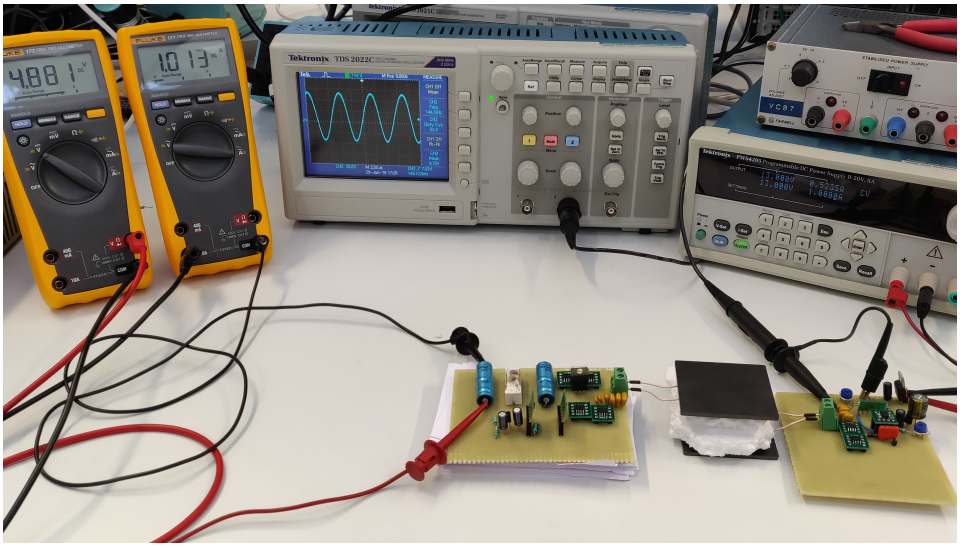

Figure 4.3: Photo of the measurement setup

The capacitors and coils have been measured using a LCR Meter HC8018. This was done to make sure the capacitance variance was accounted for in both the receiver and transmitter also considering the variance in inductance of the coils.

4.1.2. Component Validation

Coils

To validate the coils, a few things must be measured. The inductance is the obvious to be measured. This can simply be done using the LCR Meter. The real value of both coils is 25.3 μH. A little higher than the specs of the datasheet.

The second measurement is the coupling between the coils. It is useful to know what the coupling is between the coils to know what distances of operation to expect. To measure the coupling, Equation 3.3 is used. When ones leaves the receiving coils an open terminal, the equation reduces to Equation 3.5. If the voltage induced at the receiver is measured and the frequency is known, the coupling factor can be deduced through the mutual inductance. Doing this for several distances gives an idea of the coupling between the coils.

To measure the coupling at different distances, sheets of paper are used to accurately determine the spacing between the coils. The transmitting coil is powered using an amplifier at a fixed frequency. both signals can be seen in the oscilloscope. Paper does not have a significant effect on the magnetic field. After each measurement 5 sheets of paper are added, resulting in a 0.5 mm step size. A light press on the top coil ensures that no air is trapped in between the paper sheets. The setup can be seen in Figure 4.4.

The measured coupling can be seen in Figure 4.5. the data for this figure can be found in Appendix A.2.1. As can be seen in the figure, around a coupling of 0.1, the distance is around 2.5 cm.

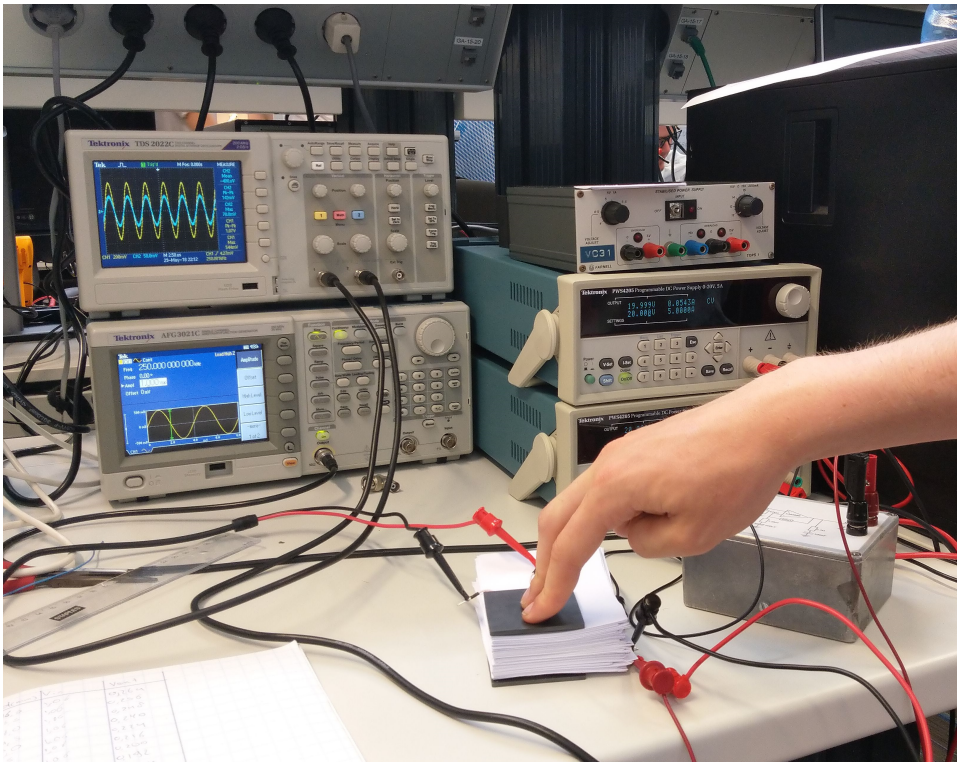

Figure 4.4: Setup used for measuring the coupling between the coils

This is well within our requirement of a minimum of two centimeters.

Capacitors

Also, the values of the capacitors were evaluated. Several capacitors were placed in series and small capacitances were added to account for the variance of the larger capacitors.

Resonant Frequency

Furthermore, it has been found that with the discussed coil and capacitance, the resonance frequency of the resonant circuit was not exactly 150 kHz. As discussed in Section 3.1.3, $\mathbf{I_2}$ (the current through the receiver resonant circuit) should lag $\mathbf{I_1}$ (the current through the transmitter resonant circuit) by $90°$. Therefore, the voltage over the tuning capacitance on the receiver side should lag the tuning capacitor voltage on the transmitter side by $90°$. This is the case at a frequency of 147.6 kHz for a coil separation distance of 20 mm. In order to get maximum power transfer, all test were ran at this resonant frequency.

4.1.3. Control

This section will validate the performance of the control: the oscillator and the gate-driver.

Oscillator

Firstly, the oscillator will be discussed. Its goal was to create a ~ 150 kHz signal with a 50% duty cycle. With the help of a potentiometer, the value of R_{SET} could be set to different values in order to create the slight variation needed to create a 147.6 kHz signal. Figure 4.6 shows the measured output of the oscillator. As expected, this is a 146.7 kHz signal with a 50% duty cycle.

The waveform has sharp edges, showing the oscillator is capable to generate the desired frequency, furthermore, the waveform oscillates between 0 and 5 volts. Thus, it behaves as expected.
The power consumption of the oscillator was measured. Only the oscillator was connected to a power supply, it consumed 20 mW.

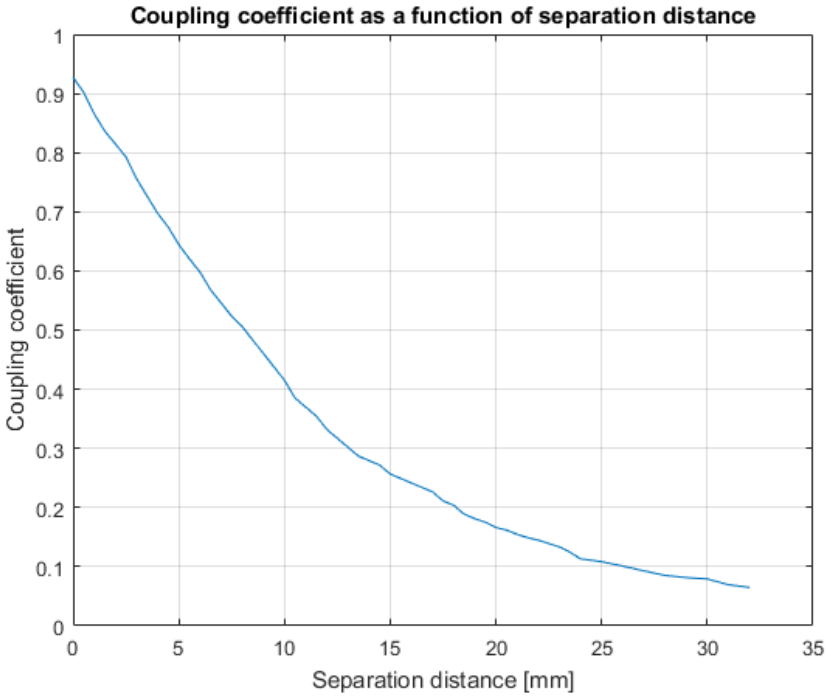

Figure 4.5: Coupling between two coils versus the separation distance

Gate-driver

Next, the gate-driver will be discussed. The goal of the gate-driver is to create a signal to drive the high-side MOSFET of the inverter and an inverted low-side gate-source signal to drive the low-side MOSFET of the inverter. The most important characteristics of the gate-driver are the deadtime and the gate-source voltage of the high-side MOSFET. Figure 4.7 shows the high and low-side outputs of the gate-driver. `CH1` shows the high-side gate signal. `CH2` shows the low-side gate signal.

The gate-driver signals are also shown in Figure 4.8 and Figure 4.9. The first of these shows the 146.7 kHz input signal of the gate-driver and both output signals as gate-source voltages of the respective MOSFETs. The second figure gives a zoomed in view on the delays between the signals. The delay between the oscillator output and the gate signal response is around 100 ns. The deadtime between the falling of one gate signal and the rising of the other is around 200 ns. Comparing these values with the calculated and simulated results, they are as expected.

The highest losses of the transmitter come from the gate-driver. The direct power consumption cannot be measured but the stated power consumption in the datasheet (and shown in Figure 3.10) does match the results in Section 4.2.

A certain artifact did catch our attention when performing these measurements. The artifact can best be seen on the low-side signal. The maximum voltage when the signal is high is not consistent for the different signals. It oscillates chaotically within a certain range. It has been determined that the cause of this is the voltage regulator for the gate-driver.

4.1.4. Inverter

The final part of the transmitter is the inverter. This uses the two gate signals to switch the source voltage to create a oscillating signal at the output. Figure 4.10 shows the gate-source signals of the high-side and low-side MOSFETs and the output signal of the inverter. It behaves as expected. The losses are small in the MOSFETs and hard to measure and are derived from the other losses in the system.

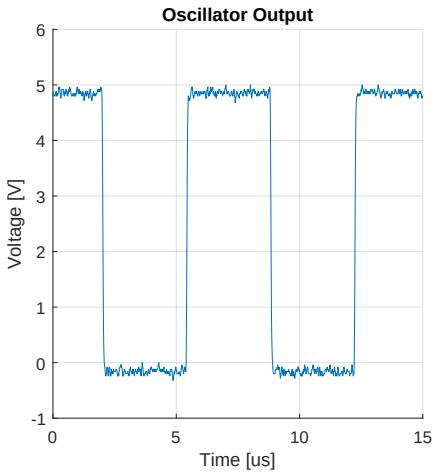

Figure 4.6: Oscillator output

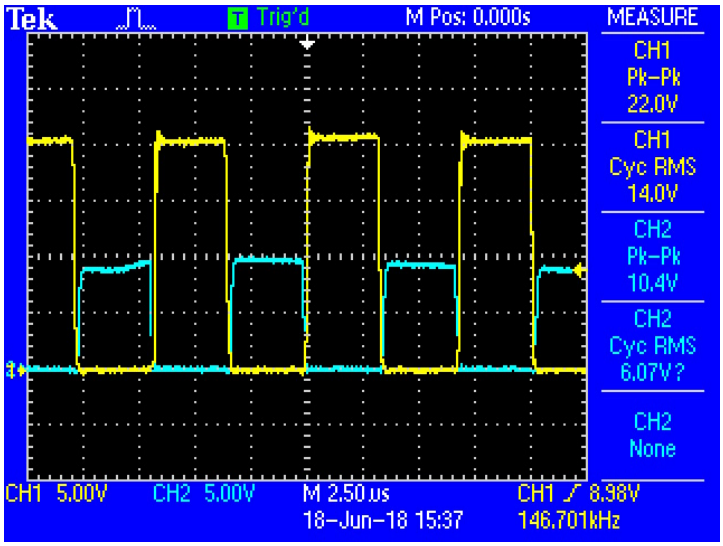

Figure 4.7: gate-driver output signals on the oscilloscope

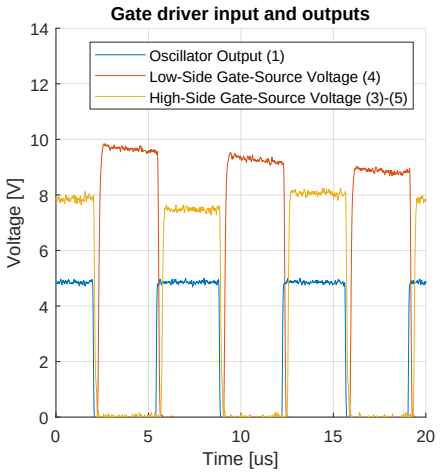

Figure 4.8: Gate-driver output signals (Signal numbers as seen in Figure 4.2)

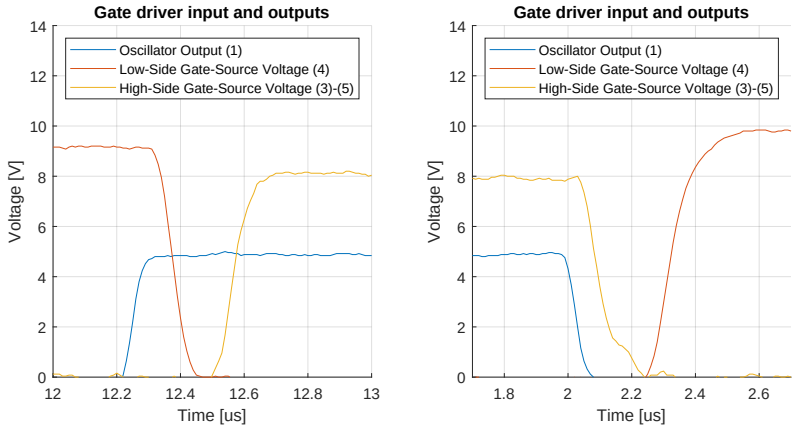

Figure 4.9: Gate-driver output signals with a view of the deadtime (Signal numbers as seen in Figure 4.2)

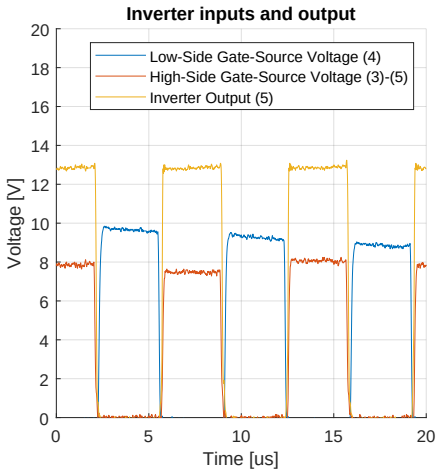

Figure 4.10: Measured inverter signals (Signal numbers as seen in Figure 4.2)

4.1.5. Resonant circuit

The resonant circuit must be tuned correctly to oscillate at its resonance peak, this will lead to maximum power transfer. This section will validate the power transfer over the airgap.

In order to obtain the amount of power transferred between the systems the amount of input and output power has to be known. For this the input/output voltage and current will be needed. As measuring this high frequency current is not possible with a regular multimeter, another method has to be found. One way to obtain the current through the resonant circuit is by measuring the voltage over the tuning capacitor. The impedance of capacitor gives a relation between the voltage over the capacitor and the current through the capacitor as shown in Equation 4.1.

$$I = \frac{V}{Z} = V \cdot (j \cdot \omega \cdot C) \quad [\mathrm{A}] \tag{4.1}$$

As the current through the capacitor is equal to the current through the resonant circuit, the instantaneous power can be calculated:

$$P = V \cdot I \quad [\mathrm{W}] \tag{4.2}$$

Figure 4.11 and Figure 4.12 show the respective input and output voltages of the resonant circuit (CH2) and the voltages over both tuning capacitors which have been used to derive the current through the transmitter and receiver side of the resonant circuit.

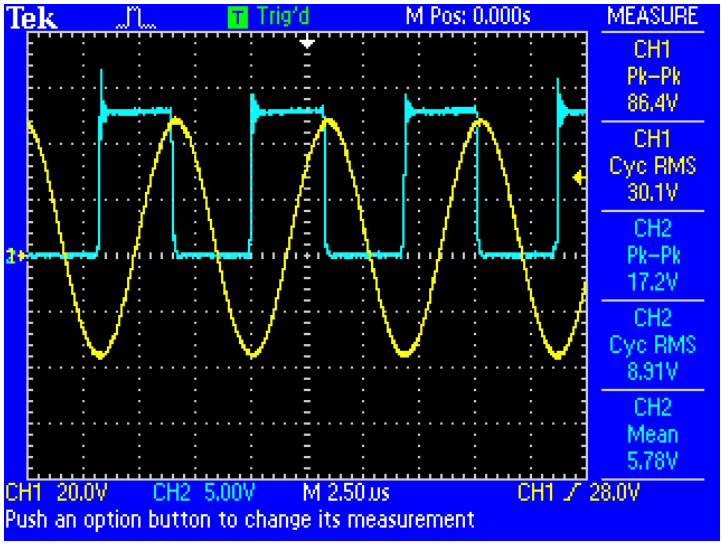

Figure 4.11: Transmitter Resonant Circuit signals from the osilloscope

Figure 4.13 shows the input voltage, current and power at the transmitter. Figure 4.14 shows the output voltage, current and power at the receiver.
The efficiency of the airgap can be seen from these figures. The input power is 6.69 W, the output power is 6.17 W. The efficiency is 92.2% over the airgap.

4.2. Efficiency Evaluation

Several of the before-mentioned results will be used to evaluate the transmitter efficiency. Operating at a coil separation distance of $20mm$, the power consumption at the power supply is $7.15W$ as the $13V$ supply delivers $0.55A$. As Figure 4.13 shows, the average power outputted by the inverter is $6.69W$. This means that the inverter and its control circuit have an efficiency of $6.69/7.15 = 93.4\%$.

Transmitter Circuit Losses

The total power lost in this circuit is $7.15 - 6.69 = 460$ mW. Of this, the power dissipation in the LTC6992 oscillator has been measured to be 20 mW. The gate-driver dissipation losses in the LM5104

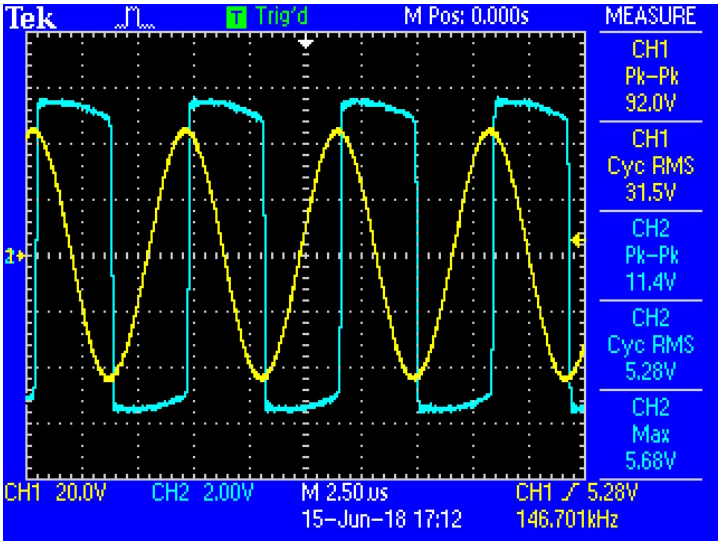

Figure 4.12: Reciever Resonant Circuit signals from the osilloscope

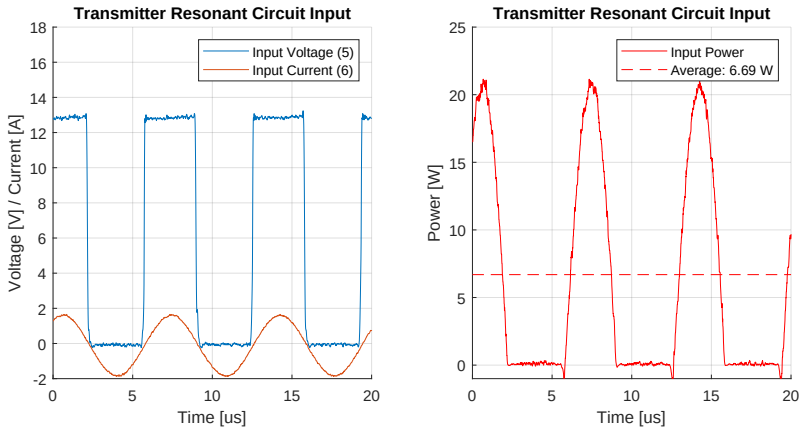

Figure 4.13: Transmitter Resonant Circuit Input (Signal numbers as seen in Figure 4.2)

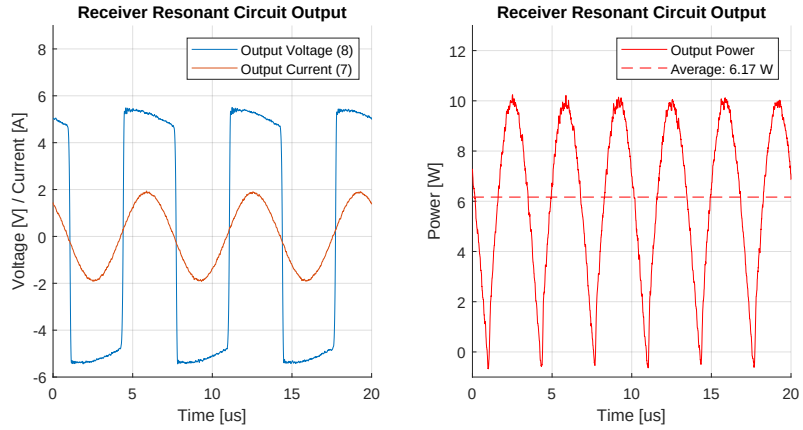

Figure 4.14: Transmitter Resonant Circuit Output (Signal numbers as seen in Figure 4.2)

are 190 mW for a 4.4 nC load at 150 kHz. The load of the two 33 nC at a gates of the MOSFETs at 10 V is equivalent to one 6.6 nF load. The power dissipation can thus be estimated 1.5 times of that of the 4.4 nF load in the datasheet and will therefore be 285 mW. Furthermore, the LM5014 has diode dissipation losses. These are 110 mW at a 4.4 nC load and can be estimated to be 165 mW at the load constructed by the two MOSFETs. The losses in the MOSFETS are estimated to be the on resistance (5 mΩ) multiplied by half of the RMS current through the resonant circuit (0.7 A). [34]

Resonant Circuit Losses

The average output power of the resonant circuit at the receiver is 6.17 W, which means the resonant circuit has an efficiency of $6.69/6.17 = 92.2\%$. Some of these power losses are due to the equivalent series resistances in the transmitter and receiver circuit. With the help of Equation 3.22 and 3.23, Equation 4.3 shows that these equivalent resistances contribute to a 390 mW power loss. As the total losses in the resonant circuit are equal to 520 mW, the losses in the magnetic field are estimated to be 130 mW.

$$P = I_{rms}^2 \cdot R_{series} = \frac{I_{peak}^2}{2} \cdot R_{series}$$

$$\Rightarrow$$

$$\begin{aligned} P_{transmitter} &= \frac{1.66^2}{2} \cdot (0.22 + 0.96) = 160 \quad [\text{mW}] \\ P_{receiver} &= \frac{1.99^2}{2} \cdot (0.22 + 0.96) = 230 \quad [\text{mW}] \\ P_{Rseries} &= 160 + 230 = 390 \quad [\text{mW}] \end{aligned} \tag{4.3}$$

Table 4.1 shows an overview of the losses and efficiencies in the whole system.

Table 4.1: Power Evaluation Table

	Power Input	Power Dissipation	Block Efficiency	Total Efficiency
Transmitter Circuit	7.15 W	460 mW	93.4 %	93.4 %
Oscillator		*20 mW*		
Gate Driver Losses		*270 mW*		
Diode Losses		*165 mW*		
Ron MOSFETs		*4 mW*		
Resonant Circuit	6.69 W	520 mW	92.2 %	86.2 %
Rseries		*390 mW*		
Magnetic Field		*130 mW*		
Receiver	6.17 W	1.17 W	81.0 %	69.9 %
Load	5 W	5 W		

Output Power Behaviour

Lastly, the behaviour of the system is analyzed for different loads and supply voltages. For this, the measurement setup is altered slightly. Figure 4.15 shows the measurement setup. The variable supply voltage input is known through the power supply and the supply current, load voltage and load current are measured. With these measurements, the total input and output power can be calculated. Furthermore, the 5 Ω load is replaced by a variable load and the voltage regulator in the rectifier is disabled. This way different output voltages can be reached to get a higher power transfer. Figure 4.16 shows the efficiency as a function of the output power. It can be seen that a higher supply voltages enables a higher output power, but also that a lower supply voltage is more efficient for the same load.
Figure 4.17 shows that the total power loss in the system has a nearly linear correlation with the supply voltage. This is caused by the linear voltage regulators in the transmitter, as their loss is linearly dependent on the voltage drop over the voltage regulators.

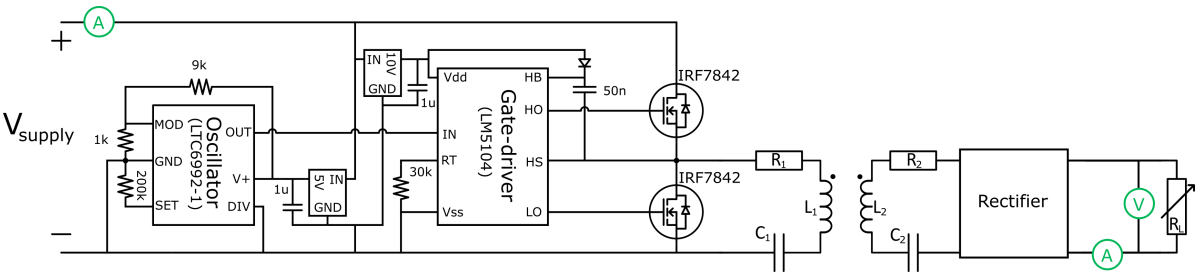

Figure 4.15: Measurement setup

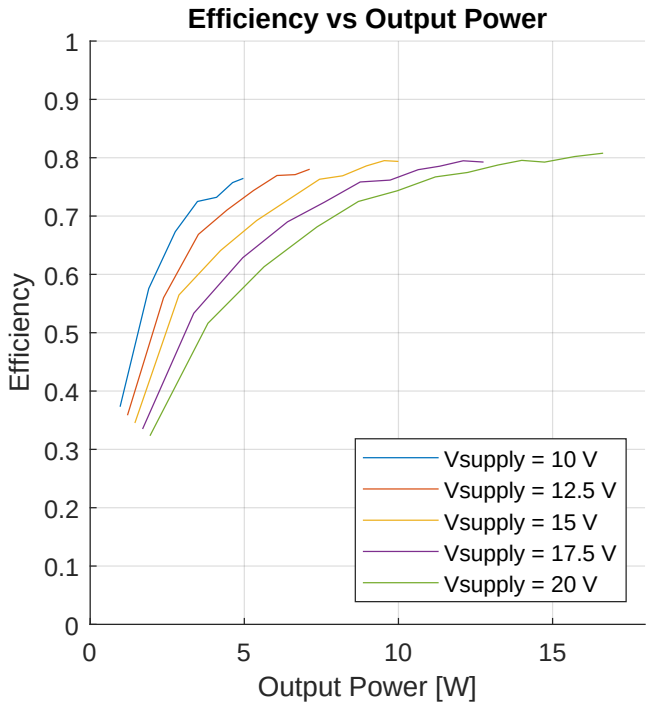

Figure 4.16: System efficiency as a function of output power

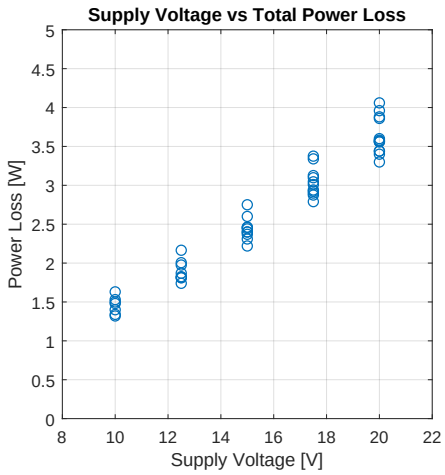

Figure 4.17: Transmitter Resonant Circuit Output

4.3. Discussion

In this discussion, the unexpected results are presented, possible flaws that have caught our attention are addressed and future work is proposed.

The most prominent surprising result that was the instability of the voltage regulator. Too little thought may have gone into choosing the voltage regulators and high frequency differential consumption through the regulator should have been investigated.

A second surprising result has been the frequency that has followed from our design optimization. With the theory stating that a higher frequency is more desirable for transferring more power, it was expected that the operation frequency would have been higher. Higher frequencies would lead to smaller components making it even more useful for hand-held devices. The Airfuel Alliance standard is an interesting option to look into, as their operating frequency is above 6 MHz.

A possible flaw in the design is found at the gate-driver. The gate-driver is powered using a 10 V voltage regulator. The gate-driver is also responsible of making sure that the high-side is turned on properly. With the variable DC supply the situation could arise that the boost of 10 volts may not be sufficient when a higher supply voltage is used. The situation is fairly robust for the power ranges that the device is currently operating in, but this could be a problem.

One of the main losses stems from the gate-charge dissipating through the gate-driver. This loss can be reduced with a technique called zero voltage switching (ZVS), with this technique the switching of the inverter MOSFETs is delayed in such a way that the gate switches at an effective zero voltage between source and gate. The capacitance of the gate is lower and will result in less losses.
Lastly, the optimum frequency for power transfer shifts due to mutual inductance at high coupling. A maximum efficiency point tracking system that tunes the frequency would be useful in making the system more robust to coupling changes while maintaining high efficiency.

5

Conclusion

The goal of this project was creating a highly efficient transmitter for a wireless power transfer system. Considering the requirements that have been stated in the PoR have been met, the project can be considered a succes. The transmitter has an efficiency of 93.4% and the resonant circuit has an efficiency of 92.2% at a distance of 2 centimeters. The system is small enough to fit in a hand-held container.

Several specific challenges have been tackled for a low power WPT system. An efficiency analysis has been done on the coupled coils to choose the best key parameters such as frequency and what tuning to apply. The inverter topology has contributed to a small control footprint and therefore reduced losses in the control. The MOSFETs have been chosen for their low on-resistance. The design has greatly contributed to the efficiency of the system.
Our measurement confirm the efficiency of the transmitter. The improvements of the system mainly lie with the gate-drivers. It has been the biggest source of losses in our system. Lower gate-charge MOSFETs would help achieving this or other gate-drivers may hold the solution.

Putting the transmitter in the scope of the whole project, the transmitter has done its job. It delivers power highly efficient. The load at the receiving end is able to receive 5 watts at 5 volts at a reasonable distance between the coils.

A

Appendix

A.1. Matlab Code

A.1.1. Efficiency Calculations

PowerResonantCircuit.m

```
clear all
close all

Ploss = zeros(10,4);

%Starting values
f = 50e3:50e3:500e3;
omega = f.*2.*pi;
L = 24e-6;
C = round(1 ./ (omega.^2 .* L), 12);
eff = 0.9; %receiver efficiency

%Rectifier resitance and power calculations
Rrect_load = 5;
Rrect_loss = 5 / eff - 5;
Prect = 5 / eff;

%% Stage 1: Frequency dependent power transfer

%Coil & Tuning Capacitor ESR
Rseries = 0.1;

for i = 1:4
    %Multiple itterations for different couplings
    k = 0.06 + 0.02 * i;
    legendStrings{i} = num2str(k,'k = %g');
    M = k * L;

    %Total receiver resistance calculation
    R = Rrect_load + Rrect_loss + Rseries;
    P = R;

    %Power loss
    Ploss(:,i) = Rseries .* P .* (1./R + R./(omega.^2.*M.^2));
end

figure(1)
subplot(121)
grid on
hold on
plot(f/1000, Ploss)
axis([50 500 0 10])
title('Power Loss in Resonant Circuit')
xlabel('Frequency [kHz]')
ylabel('Power Loss [W]')
legend(legendStrings)

subplot(122)
grid on
hold on
plot(f'/1000, Prect./(Prect+Ploss))
axis([50 500 0.5 1])
title('Efficiency in Resonant Circuit')
```

```
xlabel('Frequency [kHz]')
ylabel('Efficiency')
legend(legendStrings, 'Location', 'southeast')

printpdf2('eff1.pdf');

%% Stage 2: Including a frequency dependent equivalent series resistance

%Q factors and Dissipation Factor as found in the datasheet
Q = [115 200 235 230 200 180 160 150 135 125 115 110 105 100  95  90  88  85  80  78];
DF = 0.001;

%ESR calculation
Rseries = ( omega .* L ./ Q(1:10) ) + ( DF ./ (omega .* C) );

for i = 1:4
    %Multiple itterations for different couplings
    k = 0.06 + 0.02 * i;
    legendStrings{i} = num2str(k,'k = %g');
    M = k * L;

    %Total receiver resistance calculation
    R = Rrect_load + Rrect_loss + Rseries;
    P = R;

    %Power loss
    Ploss(:,i) = Rseries .* P .* (1./R + R./(omega.^2.*M.^2));
end

figure(2)
subplot(121)
grid on
hold on
plot(f/1000, Ploss)
axis([50 500 0 10])
title('Power Loss in Resonant Circuit')
xlabel('Frequency [kHz]')
ylabel('Power Loss [W]')
legend(legendStrings)

subplot(122)
grid on
hold on
plot(f'/1000, Prect./(Prect+Ploss))
axis([50 500 0.5 1])
title('Efficiency in Resonant Circuit')
xlabel('Frequency [kHz]')
ylabel('Efficiency')
legend(legendStrings, 'Location', 'southeast')

printpdf2('eff2.pdf');

%% Stage 3: Frequency dependent control circuit losses

%Losses as found in the datahseet (for 4.4 nF)
Pdriver = [0.08 0.14 0.18 0.25 0.33 0.39 0.48 0.55 0.63 0.70];
Pdriver = [Pdriver; Pdriver; Pdriver; Pdriver]';
Pdiode = [0.045 0.075 0.11 0.15 0.19 0.23 0.265 0.3 0.335 0.37];
Pdiode = [Pdiode; Pdiode; Pdiode; Pdiode]';

%Added to the total loss (for 6.6 nF)
%the losses are at least 1.5x larger following P=2*f*C*V^2
Ploss = Ploss + Pdriver .* 1.5 + Pdiode .* 1.5;

figure(3)
subplot(121)
grid on
hold on
plot(f/1000, Ploss)
axis([50 500 0 10])
title('Power Loss in Resonant Circuit')
xlabel('Frequency [kHz]')
ylabel('Power Loss [W]')
legend(legendStrings)

subplot(122)
grid on
hold on
plot(f'/1000, Prect./(Prect+Ploss))
axis([50 500 0.5 1])
title('Efficiency in Resonant Circuit')
xlabel('Frequency [kHz]')
ylabel('Efficiency')
legend(legendStrings, 'Location', 'southeast')
```

```
printpdf2('eff3');
```

A.2. Measurements

A.2.1. Coil Measurements

Table A.1: Measurements of the coupling between two coils

distance (mm)	V in	V out
0	1,1	1,02
0,5	1,1	0,992
1	1,1	0,952
1,5	1,1	0,92
2	1,1	0,896
2,5	1,09	0,864
3	1,09	0,824
3,5	1,09	0,792
4	1,09	0,76
4,5	1,08	0,728
5	1,08	0,696
5,5	1,07	0,664
6	1,07	0,64
6,5	1,07	0,608
7	1,07	0,584
7,5	1,07	0,56
8	1,06	0,536
8,5	1,06	0,512
9	1,06	0,488
9,5	1,06	0,464
10	1,06	0,44
10,5	1,06	0,408
11	1,06	0,392
11,5	1,06	0,376
12	1,06	0,352
12,5	1,06	0,336
13	1,06	0,32
13,5	1,06	0,304
14	1,06	0,296
14,5	1,06	0,288
15	1,06	0,272
15,5	1,06	0,264
16	1,06	0,256
16,5	1,06	0,248
17	1,06	0,24
17,5	1,06	0,224
18	1,06	0,216
18,5	1,06	0,2
19	1,06	0,192
19,5	1,05	0,184
20	1,06	0,176
20,5	1,05	0,17
21	1,06	0,164
21,5	1,06	0,158
22	1,05	0,152
22,5	1,05	0,146
23	1,05	0,14
23,5	1,06	0,132
24	1,06	0,12
25	1,06	0,115
26	1,06	0,107
27	1,06	0,0984
28	1,06	0,0904
29	1,06	0,0864
30	1,06	0,084
31	1,06	0,0736
32	1,06	0,0688

Bibliography

[1] N. Tesla, "Apparatus for transmitting electrical energy," December 1914.

[2] A. Kurs, "Power transfer through strongly coupled resonances," pp. 39–40, September 2007.

[3] K. Huang and X. Zhou, "Cutting the last wires for mobile communications by microwave power transfer," *IEEE Communications Magazine*, vol. 53, no. 6, pp. 86–93, June 2015.

[4] X. Lu, P. Wang, D. Niyato, D. I. Kim, and Z. Han, "Wireless charging technologies: Fundamentals, standards, and network applications," *IEEE Communications Surveys Tutorials*, vol. 18, no. 2, pp. 1413–1452, Secondquarter 2016.

[5] J. Sallan, J. L. Villa, A. Llombart, and J. F. Sanz, "Optimal design of icpt systems applied to electric vehicle battery charge," *IEEE Transactions on Industrial Electronics*, vol. 56, no. 6, pp. 2140–2149, June 2009.

[6] C.-S. Wang, O. H. Stielau, and G. A. Covic, "Design considerations for a contactless electric vehicle battery charger," *IEEE Transactions on Industrial Electronics*, vol. 52, no. 5, pp. 1308–1314, Oct 2005.

[7] E. S. Hochmair, "System optimization for improved accuracy in transcutaneous signal and power transmission," *IEEE Transactions on Biomedical Engineering*, vol. BME-31, no. 2, pp. 177–186, Feb 1984.

[8] D. van Wageningen and T. Staring, "The qi wireless power standard," in *Proceedings of 14th International Power Electronics and Motion Control Conference EPE-PEMC 2010*, Sept 2010, pp. S15–25–S15–32.

[9] "Airfuel alliance," https://www.airfuel.org/, accessed: 2018-04-26.

[10] G. Yang, M. R. V. Moghadam, and R. Zhang, "Magnetic mimo signal processing and optimization for wireless power transfer," *IEEE Transactions on Signal Processing*, vol. 65, no. 11, pp. 2860–2874, June 2017.

[11] F. Jolani, Y. Yu, and Z. Chen, "A planar magnetically coupled resonant wireless power transfer system using printed spiral coils," *IEEE Antennas and Wireless Propagation Letters*, vol. 13, pp. 1648–1651, 2014.

[12] H. Li, X. Yang, K. Wang, and X. Dong, "Study on efficiency maximization design principles for wireless power transfer system using magnetic resonant coupling," in *2013 IEEE ECCE Asia Downunder*, June 2013, pp. 888–892.

[13] M. Kiani and M. Ghovanloo, "The circuit theory behind coupled-mode magnetic resonance-based wireless power transmission," *IEEE Transactions on Circuits and Systems I: Regular Papers*, vol. 59, no. 9, pp. 2065–2074, Sept 2012.

[14] S. Wang and D. Gao, "Power transfer efficiency analysis of the 4-coil wireless power transfer system based on circuit theory and coupled-mode theory," in *2016 IEEE 11th Conference on Industrial Electronics and Applications (ICIEA)*, June 2016, pp. 1230–1234.

[15] A. K. RamRakhyani, S. Mirabbasi, and M. Chiao, "Design and optimization of resonance-based efficient wireless power delivery systems for biomedical implants," *IEEE Transactions on Biomedical Circuits and Systems*, vol. 5, no. 1, pp. 48–63, Feb 2011.

[16] T. Imura and Y. Hori, "Maximizing air gap and efficiency of magnetic resonant coupling for wireless power transfer using equivalent circuit and neumann formula," *IEEE Transactions on Industrial Electronics*, vol. 58, no. 10, pp. 4746–4752, Oct 2011.

[17] S. Y. R. Hui, W. Zhong, and C. K. Lee, "A critical review of recent progress in mid-range wireless power transfer," *IEEE Transactions on Power Electronics*, vol. 29, no. 9, pp. 4500–4511, Sept 2014.

[18] K. O. Gurov and E. A. Mindubaev, "Geometry influence on the coils mutual inductance in the transcutaneous energy transfer system," in *2018 IEEE Conference of Russian Young Researchers in Electrical and Electronic Engineering (EIConRus)*, Jan 2018, pp. 1894–1896.

[19] M. Kim, H. P. Park, and J. H. Jung, "Coil misalignment compensation algorithm for single-stage inductive wireless power transfer system using model-based approach," in *2018 IEEE Applied Power Electronics Conference and Exposition (APEC)*, March 2018, pp. 3057–3061.

[20] X. Li, X. Dai, Y. Li, Y. Sun, Z. Ye, and Z. Wang, "Coupling coefficient identification for maximum power transfer in wpt system via impedance matching," in *2016 IEEE PELS Workshop on Emerging Technologies: Wireless Power Transfer (WoW)*, Oct 2016, pp. 27–30.

[21] M. Pinuela, D. C. Yates, S. Lucyszyn, and P. D. Mitcheson, "Maximizing dc-to-load efficiency for inductive power transfer," *IEEE Transactions on Power Electronics*, vol. 28, no. 5, pp. 2437–2447, May 2013.

[22] S. Chopra and P. Bauer, "Analysis and design considerations for a contactless power transfer system," in *2011 IEEE 33rd International Telecommunications Energy Conference (INTELEC)*, Oct 2011, pp. 1–6.

[23] T. Koyama, T. Honjo, M. Ishihara, K. Umetani, and E. Hiraki, "Simple self-driven synchronous rectifier for resonant inductive coupling wireless power transfer," in *2017 IEEE International Telecommunications Energy Conference (INTELEC)*, Oct 2017, pp. 363–368.

[24] C. H. K. Jensen, F. M. Spliid, J. C. Hertel, Y. Nour, T. G. Zsurzsan, and A. Knott, "Resonant full-bridge synchronous rectifier utilizing 15 v gan transistors for wireless power transfer applications following airfuel standard operating at 6.78 mhz," in *2018 IEEE Applied Power Electronics Conference and Exposition (APEC)*, March 2018, pp. 3131–3137.

[25] F. Liu, W. Lei, T. Wang, C. Nie, and Y. Wang, "A phase-shift soft-switching control strategy for dual active wireless power transfer system," in *2017 IEEE Energy Conversion Congress and Exposition (ECCE)*, Oct 2017, pp. 2573–2578.

[26] H. Li, J. Fang, S. Chen, K. Wang, and Y. Tang, "Pulse density modulation for maximum efficiency point tracking of wireless power transfer systems," *IEEE Transactions on Power Electronics*, vol. 33, no. 6, pp. 5492–5501, June 2018.

[27] H. Li, J. Fang, S. Chen, Y. Tang, and K. Wang, "A pulse density modulation method for zvs full-bridge converters in wireless power transfer systems," in *2018 IEEE Applied Power Electronics Conference and Exposition (APEC)*, March 2018, pp. 3143–3148.

[28] "Aanbeveling van de raad van 12 juli 1999 betreffende de beperking van blootstelling van de bevolking aan elektromagnetische velden van 0 hz — 300 ghz," July 1999, (1999/519/EG).

[29] *760308110 Coil Datasheet*, April 2017.

[30] H. A. Wheeler, "Formulas for the skin effect," *Proceedings of the IRE*, vol. 30, no. 9, pp. 412–424, Sept 1942.

[31] L. Jinliang, D. Qijun, H. Wenshan, and Z. Hong, "Research on quality factor of the coils in wireless power transfer system based on magnetic coupling resonance," in *2017 IEEE PELS Workshop on Emerging Technologies: Wireless Power Transfer (WoW)*, May 2017, pp. 123–127.

[32] *LTC6992 TimerBlox: Voltage-Controlled Pulse Width Modulator (PWM) - Datasheet*, Januari 2012.

[33] *250 mA Low Quiescent Current LDO Regulator - Datasheet*, November 2010.

[34] *LM5104 High-Voltage Half-Bridge Gate Driver With Adaptive Delay - Datasheet*, December 2014.

[35] *TL750L10 low-dropout voltage regulator - Datasheet*, September 2009.

[36] D. Neamen, *Semiconductor Physics And Devices*, 3rd ed. New York, NY, USA: McGraw-Hill, Inc., 2003.

[37] *RF7842 HEXFET Power MOSFET - Datasheet*, April 2004.